Title: Candidate gene scan for Single Nucleotide Polymorphisms involved in the determination of normal variability in human craniofacial morphology

Authors: Mark Barash[1,2*], Philipp E. Bayer[3,4], Angela van Daal[2]

Affiliations:

[1]School of Mathematical and Physical Sciences, Centre for Forensic Sciences, Faculty of Science, University of Technology Sydney, Sydney, NSW, Australia

[2]Faculty of Health Sciences and Medicine, Bond University, Gold Coast, QLD, Australia

[3]School of Agriculture and Food Sciences, The University of Queensland, Brisbane, QLD, Australia

[4]Australian Centre for Plant Functional Genomics, The University of Queensland, Brisbane, QLD, Australia

Emails: Mark Barash mark.barash@uts.edu.au; Philipp E. Bayer philipp.bayer@uqconnect.edu.au; Angela van Daal vandaalconsult@gmail.com

* Corresponding author email: mark.barash@uts.edu.au

* Corresponding author postal address: Centre for Forensic Sciences, School of Mathematical and Physical Sciences, Faculty of Science University of Technology Sydney, Building 4, Thomas St, Broadway NSW 2007, Australia.

Abstract

Despite intensive research on genetics of the craniofacial morphology using animal models and human craniofacial syndromes, the genetic variation that underpins normal human facial appearance is still largely elusive. Recent development of novel digital methods for capturing the complexity of craniofacial morphology in conjunction with high-throughput genotyping methods, show great promise for unravelling the genetic basis of such a complex trait.

As a part of our efforts on detecting genomic variants affecting normal craniofacial appearance, we have implemented a candidate gene approach by selecting 1,201 single nucleotide polymorphisms (SNPs) and 4,732 tag SNPs in over 170 candidate genes and intergenic regions. We used 3-dimentional (3D) facial scans and direct cranial measurements of 587 volunteers to calculate 104 craniofacial phenotypes. Following genotyping by massively parallel sequencing, genetic associations between 2,332 genetic markers and 104 craniofacial phenotypes were tested.

An application of a Bonferroni–corrected genome–wide significance threshold produced significant associations between five craniofacial traits and six SNPs. Specifically, associations of nasal width with rs8035124 (15q26.1), cephalic index with rs16830498 (2q23.3), nasal index with rs37369 (5q13.2), transverse nasal prominence angle with rs59037879 (10p11.23) and rs10512572 (17q24.3), and principal component explaining 73.3% of all the craniofacial phenotypes, with rs37369 (5p13.2) and rs390345 (14q31.3) were observed.

Due to over-conservative nature of the Bonferroni correction, we also report all the associations that reached the traditional genome-wide p-value threshold (<5.00E-08) as suggestive. Based on the genome-wide threshold, 8 craniofacial phenotypes demonstrated significant associations with 34 intergenic and extragenic SNPs. The majority of associations are novel, except *PAX3* and *COL11A1* genes, which were previously reported to affect normal craniofacial variation.

This study identified the largest number of genetic variants associated with normal variation of craniofacial morphology to date by using a candidate gene approach, including confirmation of the two previously reported genes. These results enhance our understanding of the genetics that determines normal variation in craniofacial morphology and will be of particular value in medical and forensic fields.

Keywords

SNPs, single nucleotide polymorphisms, craniofacial, facial appearance, embryogenetics forensic DNA phenotyping, facial reconstruction.

Author Summary

There is a remarkable variety of human facial appearances, almost exclusively the result of genetic differences, as exemplified by the striking resemblance of identical twins. However, the genes and specific genetic variants that affect the size and shape of the cranium and the soft facial tissue features are largely unknown. Numerous studies on animal models and human craniofacial disorders have identified a large number of genes, which may regulate normal craniofacial embryonic development.

In this study we implemented a targeted candidate gene approach to select more than 1,200 polymorphisms in over 170 genes that are likely to be involved in craniofacial development and morphology. These markers were genotyped in 587 DNA samples using massively parallel sequencing and analysed for association with 104 traits generated from 3-dimensional facial images and direct craniofacial measurements. Genetic associations (p-values<5.00E-08) were observed between 8 craniofacial traits and 34 single nucleotide polymorphisms (SNPs), including two previously described genes and 26 novel candidate genes and intergenic regions. This comprehensive candidate gene study has uncovered the largest number of novel genetic variants affecting normal facial appearance to date. These results will appreciably extend our understanding of the normal and abnormal embryonic development and impact our ability to predict the appearance of an individual from a DNA sample in forensic criminal investigations and missing person cases.

Introduction

The human face is probably the most commonly used descriptor of a person and has an extraordinary role in human evolution, social interactions, clinical applications as well as forensic investigations. The influence of genes on facial appearance can be seen in the

striking resemblance of monozygotic twins as well as amongst first degree relatives, indicating a high heritability [1, 2].

Uncovering the genetic background for regulation of craniofacial morphology is not a trivial task. Human craniofacial development is a complex multistep process, involving numerous signalling cascades of factors that control neural crest development, followed by a number of epithelial-mesenchymal interactions that control outgrowth, patterning and skeletal differentiation, as reviewed by Sperber et. al. [2]. The mechanisms involved in this process include various gene expression and protein translation patterns, which regulate cell migration, positioning and selective apoptosis, subsequently leading to development of specific facial prominences. These events are precisely timed and are under hormonal and metabolic control. Most facial features of the human embryo are recognizable from as early as 6 weeks post conception, developing rapidly *in utero* and continuing to develop during childhood and adolescence [3, 4]. Development of the face and brain are interconnected and occur at the same time as limb formation. Facial malformations therefore, frequently occur with brain and limb abnormalities and vice versa. Genetic regulation of craniofacial development involves several key morphogenic factors such as *HOX*, *WNT*, *BMP*, *FGF* as well as hundreds of other genes and intergenic regulatory regions, incorporating numerous polymorphisms [2]. The SNPs involved in craniofacial diseases may in fact influence the extraordinary variety of human facial appearances, in the same way that genes responsible for albinism have been shown to be involved in normal pigmentation phenotypes [5]. Additionally, non-genetic components such as nutrition, climate and socio-economic environment may also affect human facial morphology via epigenetic regulation of transcription, translation and other cellular mechanics. To date, both the genetic and even more so, the epigenetic regulation of craniofacial morphology shaping are poorly understood.

The genetic basis of craniofacial morphogenesis has been explored in numerous animal models with multiple loci shown to be involved [2]. The majority of human studies in this field have focused on the genetics of various craniofacial disorders such as craniosynostosis and cleft lip/palate [6, 7], which may provide a link to regulation of normal variation of the craniofacial phenotype, as for example observed between cleft-affected offspring and the increase of facial width seen in non-affected parents [8]. These studies have identified several genes with numerous genetic variants that may contribute to normal variation of different facial features, such as cephalic index, bizygomatic distance and nasal area measurements [9-11]. Studies of other congenital disorders involving manifestation of craniofacial

abnormalities such as Alagille syndrome (*JAG1* and *NOTCH2* gene mutations), Down syndrome (chromosome 21 trisomy - multiple genes), Floating-Harbor syndrome (*SRCAP* gene mutations) and Noonan syndrome (mutations in various genes such as *PTPN11* and *RAF1*) provide additional information on the candidate genes potentially involved in normal craniofacial development [12-17].

In recent years, new digital technologies such as 3-Dimentional laser imaging have been used in numerous anthropometric studies. 3-D laser imaging allows accurate and rapid capture of facial morphology, providing a better alternative to traditional manual measurements of craniofacial distances [18-20]. The high-throughput genotyping technologies and digital methods for capturing facial morphology have been used in a number of recent studies that demonstrated a link between normal facial variation and specific genetic polymorphisms [21-23]. Despite these promising results, our current knowledge of craniofacial genetics is sparse.

This study aims to further define the polymorphisms associated with normal facial variation using a candidate gene approach. The advantage of a candidate gene approach over previous genome wide association studies (GWAS) is that it focuses on genes, which have previously been associated with craniofacial embryogenesis or inherited craniofacial syndromes, rather than screening hundreds of thousands of non-specific markers. This approach aims to increase the chances of finding significant associations between SNPs and visible traits and requires fewer samples for robust association analysis [24, 25].

In the current study, 32 anthropometric landmarks were recorded from 3-D facial scans of 587 volunteers from general Australian population (Gold Coast, Queensland). Additionally, three direct cranial measurements using a calliper were made and two facial traits (ear lobe and eye lid morphology) were recorded. Both the direct measurements and the Cartesian coordinates of the anthropometric landmarks were used to calculate 92 craniofacial distances. The calculation of 10 principal components based on the craniofacial measurements was performed in order to obtain a more simplified representation of the facial shape. The associations between 104 of the total craniofacial traits and 2,332 genetic markers were tested.

This research aims to assist in uncovering the genetic basis of normal craniofacial morphology variation and will enhance our understanding of craniofacial embryogenetics. These findings could be useful in building models to predict facial appearance from a forensic DNA sample where no suspect has been identified, thereby providing valuable

152 investigative leads. It could also assist in identifying skeletal remains by allowing more
153 accurate facial reconstructions.

154

155 Results

156

157 3D measurements precision study

158 In the last decade 3D scanning systems have been extensively used in anthropometric
159 studies as well as in medical research [18, 20, 64, 65]. The Minolta Vivid V910 3D scanner
160 has been demonstrated to have accuracy to a level of 1.9 ± 0.8 mm [66] and 0.56 ± 0.25 mm
161 [67], making it suitable for the present study since it should provide an accurate
162 representation of facial morphology. However, the allocation of anthropometric facial
163 landmarks can be challenging, especially when tissue palpating is not possible.
164 Reproducibility of the landmark precision was assessed on fifteen 3D facial images through
165 assessment of 85 facial measurements, including linear and angular distances and ratios
166 between the linear distances at two separate times. The period between the analyses varied
167 from one to six months. The mean difference (MD) was calculated as the discrepancy
168 between the first and the second measurement. The measurement error (ME) was calculated
169 as the standard deviation of the MD divided by square root of 2 ($ME=SD(MD/\sqrt{2})$).

170 In general, the nasal area distances, which involved nasion, pronasale, subnasale and alare
171 landmarks showed greater reproducibility, while the measurements involving paired
172 landmarks, such as gonion and zygion demonstrated higher variance. This result can be
173 explained by easier allocation of nasal area landmarks, compared with gonion and zygion
174 [29]. Overall the median difference (MD) between two measurements for linear distances in
175 15 images ranged between 0.76 mm (ME ±0.27) and 2.80 mm (ME ±0.99); for angular
176 distances between 0.38 mm (ME ±0.96) and 3.75 mm (ME ±0.40) and for facial indices
177 (ratios) between 0.46 mm (ME ±1.08) and 2.98 mm (ME ±1.95) respectively. The lower
178 reproducibility in the angular distances and indices can be explained by a higher number of
179 landmarks (hence variability in allocation of x, y and z coordinates) needed for their
180 calculation (three and four landmarks respectively). Nevertheless, our findings are concordant
181 with the published results, which observed variance of 0.19 mm to 3.49 mm with a ME range
182 of 0.55 mm to 3.34 mm for each landmark [19, 68].

Candidate genes search and sequencing data quality control

The search for candidate genes and SNPs potentially involved in influencing normal craniofacial morphology variation initially focused on searching for genes involved in normal or abnormal craniofacial variation in humans and model organisms (Supplemental Table S1). As a complementary approach, a search for genetic markers with high Fst values (≥0.45) was implemented, based on the rationale that genes involved in craniofacial morphology regulation are likely to display significant differences in allele frequencies across populations.

The first approach has mainly focused on the Mouse Genome Informatics (MGI) database search using the keyword 'craniofacial mutants' and additional resources such as Online Mendelian Inheritance in Man (OMIM), GeneCards and AmiGO, using the keywords such as "craniofacial", "craniofacial mutants", "craniofacial anomalies", "craniofacial dimorphism" and "facial morphology" (a detailed list of used resources is summarized in Supplemental Appendix S1). This search revealed a list of 2,891 genotypes and 7,956 annotations. A search of the 'abnormal facial morphology' sub-category resulted in 1,492 genotypes and 2,889 annotations. The final search of the 'abnormal nose morphology' of the previous sub-category revealed 219 genotypes with 310 annotations, representing approximately 150 genes.

In parallel, a search for high Fst markers, using previously published AIMs and web tools, such as ENGINES, resulted in identification of additional targets, for a total of 1,088 genes and intergenic regions (a detailed list of used resources is summarized in Supplemental Appendix S1).

However, manual examination revealed that 592 of these genes showed no apparent link with normal craniofacial development or malformations and were therefore excluded. The remaining 496 regions were further screened for non-synonymous and potentially functional SNPs, as well as SNPs with high population differentiation, which resulted in the shortlist of 269 genes and intergenic regions.

Subsequent analysis of these 269 genes/regions for functional annotation using the AmiGO Gene Onthology server [57], resulted in 177 candidate genes/regions, possessing 1,319 genetic markers involved in various stages of human embryonic development, including: embryonic morphogenesis, sensory organ development, tissue development, pattern

specification process, tissue morphogenesis, ear development, tube morphogenesis, epithelium development, chordate embryonic development and morphogenesis of an epithelium (Supplemental Appendix S1). Notably, the majority of these markers are located in introns and intergenic regions.

In terms of molecular function, AmiGO showed that craniofacial candidate markers might be involved in a range of regulatory activities including: protein dimerization activity, chromatin binding, regulatory region DNA binding, sequence-specific DNA binding RNA polymerase II transcription factor activity, sequence-specific distal enhancer binding activity, heparin binding, RNA polymerase II core promoter proximal region sequence-specific DNA binding transcription factor activity involved in positive regulation of transcription, BMP receptor binding and transmembrane receptor protein serine/threonine kinase binding (Supplemental Appendix S1).

Subsequent analysis of candidate SNPs for mouse phenotype associations confirmed that orthologous candidate markers were previously detected in mouse models displaying abnormal morphology of the skeleton, head, viscerocranium and facial area, as well as specific malformations of the eye, ear, jaw, palate, limbs, digits and tail (data not shown).

In additional to craniofacial candidate SNPs, 522 markers, previously shown to be associated with pigmentation traits, such as eye, skin and hair colour were selected from the relevant literature. These markers were used to validate the results of the genetic association analyses of craniofacial traits.

The final candidate marker list was analysed using the GREAT platform to visualize the genomic context of amplicons covering targeted SNPs [69]. The analysis revealed that almost 99% of the genomic regions (which may cover multiple markers) are associated with one or two genes with approximately 62% of genomic regions located 0-500 kb downstream of a transcription start site (data not shown).

Targeted massively parallel sequencing of the 587 samples resulted in 9,051 genetic markers, with the majority of markers (>5,000) represented by rare polymorphisms of ≤1% minor allele frequency (MAF) (data not shown). The difference between the initial hot-spot SNP panel of candidate markers (n=6,945) and the actual sequencing output (n=9,051) was a result of identification of potentially novel and rare markers in individual DNA samples. Three of the 587 samples, did not produce high quality genotypes because of poor DNA quality or unsuccessful library and template preparation.

The SNPs were filtered by sequencing quality and by MAF. Data quality control was performed by removing markers of low genotype quality (GQ>10) and sequencing depth (DP>10X), which resulted in 8,518 markers (Supplemental Appendix S2). Further filtering of markers using a 2% MAF cut-off resulted in 3,075 markers (Supplemental Appendix S2). The decision to apply a slightly more stringent MAF threshold (2%) was made because of the sample size (n=587) and to reduce potential bias from rare SNPs (1% MAF). Since this may reduce the power of analysis, we analysed and compared both datasets and did not observed any significant difference. Additional filtering based on the HWE threshold of p-value ≥0.01 resulted in 2,332 markers. The mean sequencing depth for significantly associated markers in this study was 58 fold (±48.9 SD).

Genetic association study

The association analyses were performed using a linear regression model, incorporating EIGENSTRAT-generated PCA as well as sex and BMI as covariates. The use of covariates in the statistical analysis aimed to reduce the risk of introducing confounding effects, which can result in false positive associations. While sexual dimorphism in the craniofacial morphology is well-known [70], BMI will also likely affect certain craniofacial traits, since the soft facial tissue may change significantly with weight gain or loss. Despite that, this potential confounding factor has to date been disregarded in association studies of normal craniofacial morphology. Age was not considered a significant covariate, given that average age of the subjects in this study was 27 (±8.9 SD). Nevertheless, the potential effect of age as a cofactor was assessed on three craniofacial traits and found to be not significant (data not shown).

While the majority of current GWA studies rely on a p-value <5.00E-08 significance threshold, some publications suggest this threshold may be too stringent, especially for complex traits that are regulated by a large number of small effect alleles [75, 76]. In contrast to GWAS, candidate gene studies undertake a more focused genetic strategy, concentrating on a relatively limited number of putative markers. As this study analysed a significantly lower number of SNPs than usual GWA-studies, we could use a higher p-value cut-off since the smaller sample size means the probability of false positive at extremely low p-values is itself lower. Nevertheless, we decided to keep the traditional GWAS p-value significance threshold (<5.00E-08) in order to reduce the possibility of detecting false positive results.

In addition, we subsequently applied a more stringent Bonferroni – corrected threshold in order to minimize the chance of detecting spurious associations. Following the association analysis of 104 craniofacial phenotypes with 2,332 genetic markers, the significance threshold based on the Bonferroni correction with a desired α of 0.05 would be 2.06E-07 (=0.05/(2,332*104)).

However, it should be emphasized that the Bonferroni correction is widely considered over-conservative, especially in the case of complex phenotypic traits with small individual effects of each allele. Considering that our results confirm the previously published findings, we believe the GWAS p-value threshold is conservative enough to avoid or at least significantly reduce potentially spurious associations. Following this rationale, we report all the variants, which met the unadjusted genome-wide association p-value threshold as suggestive. We believe these findings are useful for the future studies focusing on genetics of normal craniofacial morphology.

The results of the association analyses of the craniofacial traits are summarized in Table 1 and Supplemental Figs. S1-S16. In general, following the application of a stringent Bonferroni-corrected GWAS threshold (adjusted p-value <1.6E-07), we observed five craniofacial traits being associated with six genomic markers. Specifically, nasal width with rs8035124 (p-value 1.74E-07, Beta=1.366, SE=0.209), cephalic index with rs16830498 (p-value 8.67E-08, Beta=3.005, SE=0.4518), nasal index with rs37369 (p-value 1.43E-07, Beta=4.025, SE=0.6124), transverse nasal prominence angle with rs59037879 (p-value 6.07E-09, Beta=4.765, SE=0.6685) and rs10512572 (p-value 1.57E-08, Beta=1.505, SE=0.2171), and principal component (EV=1391.99) with rs37369 (p-value 2.85E-08, Beta=-0.021, SE=0.003079) and rs390345 (p-value 8.55E-08, Beta=-0.0184, SE=0.002768). The polymorphisms: rs16830498, rs59037879 and rs390345 are intronic variants in *CACNB4*, *ZEB1* and *FOXN3* respectively; rs37369 is a missense mutation in the *AGXT2* gene and rs8035124 and rs10512572 are intergenic variants in 15q12.2 and 17q21.33 chromosomal locations respectively.

308 **Table 1. Results of genetic association analyses between candidate SNPs and craniofacial traits, including all genomic markers reached the**
309 **unadjusted p-value threshold of <5.00E-08.**

gene/intergenic region	rs#	chromosomal location	observed alleles	MAF	genomic annotation	UNADJ	BONF	HOLM	BETA	SE
				nasal width (al-al)						
15q26.1	**rs8035124**	**15:92105708**	**A/C**	**3.08E-01**	**intergenic**	**1.52E-10**	**1.74E-07**	**1.74E-07**	**1.37E+00**	**2.09E-01**
EYA2	rs58733120	20:45803852	C/G	2.29E-02	intronic	5.37E-10	6.15E-07	6.14E-07	4.98E+00	7.86E-01
RP11-494M8.4	rs1482795	11:7850345	C/T	1.71E-01	intergenic	7.68E-10	8.78E-07	8.77E-07	1.56E+00	2.48E-01
AGXT2	rs37369	5:35037115	C/T	1.77E-01	missense	1.04E-09	1.19E-06	1.19E-06	1.51E+00	2.43E-01
9q22.32 (downstream to PTCH1)	rs57585041	9:98205221	G/T	2.95E-02	intergenic	6.05E-09	6.92E-06	6.90E-06	3.63E+00	6.13E-01
EYA1	rs79867447	8:72127562	C/T	2.19E-02	intronic	3.92E-08	4.49E-05	4.47E-05	4.89E+00	8.73E-01
				nasal tip protrusion (sn-prn)						
17q24.3	rs10512572	17:69512099	A/G	1.67E-01	intergenic	2.22E-08	2.54E-05	2.54E-05	-9.43E-01	1.66E-01
				cephalic index						
CACNB4	**rs16830498**	**2:152814028**	**C/T**	**9.06E-02**	**intronic**	**7.57E-11**	**8.67E-08**	**8.67E-08**	**3.01E+00**	**4.52E-01**
MYO5A	rs2290332	15:52611451	A/G	2.19E-01	synonymous	5.56E-10	6.37E-07	6.37E-07	1.99E+00	3.15E-01
ZEB1	rs59037879	10:31745993	A/T	2.49E-02	intronic	6.27E-10	7.18E-07	7.17E-07	6.24E+00	9.85E-01
COL11A1	rs4908280	1:103420759	G/T	3.14E-01	intronic	1.66E-09	1.91E-06	1.90E-06	-1.70E+00	2.77E-01
EYA1	rs1481800	8:72131426	A/G	3.62E-01	intronic	2.07E-09	2.37E-06	2.36E-06	1.66E+00	2.72E-01
TEX41	rs10496971	2:145769943	G/T	1.87E-01	intronic	5.32E-09	6.09E-06	6.06E-06	1.99E+00	3.36E-01
PCDH15	rs10825273	10:55968685	C/T	2.82E-01	intronic	9.93E-09	1.14E-05	1.13E-05	1.71E+00	2.94E-01
COL11A1	rs11164649	1:103444679	G/T	3.15E-01	intronic	1.70E-08	1.95E-05	1.94E-05	-1.63E+00	2.85E-01
5q14.3	rs373272	5:84818656	A/G	4.22E-01	intergenic	2.40E-08	2.75E-05	2.73E-05	1.53E+00	2.69E-01
				nasal index (al-al/n-sn)						
AGXT2	**rs37369**	**5:35037115**	**C/T**	**1.77E-01**	**missense**	**1.25E-10**	**1.43E-07**	**1.43E-07**	**4.03E+00**	**6.12E-01**
EYA2	rs58733120	20:45803852	C/G	2.29E-02	intronic	9.46E-09	1.08E-05	1.08E-05	1.18E+01	2.03E+00
RP11-408B11.2	rs7311798	12:85808703	C/T	9.71E-02	intergenic	1.77E-08	2.02E-05	2.02E-05	5.00E+00	8.73E-01
11q15.4	rs1482795	11:7850345	C/T	1.71E-01	intergenic	1.83E-08	2.09E-05	2.09E-05	3.66E+00	6.40E-01
EYA1	rs79867447	8:72127562	C/T	2.19E-02	intronic	3.53E-08	4.03E-05	4.02E-05	1.26E+01	2.24E+00

nose-face width index (al-al/zy-zy)										
EYA1	rs79867447	8:72127562	C/T	2.19E-02	intronic	1.10E-09	1.26E-06	1.26E-06	3.75E+00	6.02E-01
EYA2	rs58733120	20:45803852	C/G	2.29E-02	intronic	3.38E-09	3.86E-06	3.86E-06	3.25E+00	5.39E-01
EGFR	rs17335905	7:55131384	C/T	3.30E-02	intronic	4.74E-08	5.42E-05	5.41E-05	2.26E+00	4.07E-01
nasolabial angle (prn-sn-ls)										
SMAD1	rs17020235	4:146418167	A/G	3.59E-02	intronic	2.07E-09	2.36E-06	2.36E-06	-1.15E+01	1.87E+00
transverse nasal prominence angle (t-l)-prn-(t-r)										
ZEB1	**rs59037879**	**10:31745993**	**A/T**	**2.49E-02**	**intronic**	**5.31E-12**	**6.07E-09**	**6.07E-09**	**4.77E+00**	**6.69E-01**
17q24.3	**rs10512572**	**17:69512099**	**A/G**	**1.67E-01**	**intergenic**	**1.38E-11**	**1.57E-08**	**1.57E-08**	**1.51E+00**	**2.17E-01**
AGXT2	rs37369	5:35037115	C/T	1.77E-01	missense	1.46E-09	1.66E-06	1.66E-06	1.31E+00	2.12E-01
LMNA	rs12076700	1:156055099	C/G	2.28E-01	intronic	1.54E-09	1.75E-06	1.75E-06	1.18E+00	1.92E-01
FAM49A	rs6741412	2:16815759	C/G	3.99E-01	intronic	2.75E-09	3.14E-06	3.13E-06	9.96E-01	1.64E-01
TEX41	rs10496971	2:145769943	G/T	1.87E-01	intronic	5.52E-09	6.30E-06	6.27E-06	1.27E+00	2.14E-01
RTTN	rs74884233	18:67813813	A/G	2.59E-02	intronic	1.20E-08	1.37E-05	1.37E-05	3.07E+00	5.30E-01
AC073218.1	rs892458	2:34667749	C/T	4.97E-01	intergenic	1.73E-08	1.98E-05	1.97E-05	9.61E-01	1.68E-01
PAX3	rs2289266	2:223089431	G/T	1.23E-01	intronic	1.95E-08	2.23E-05	2.21E-05	1.58E+00	2.76E-01
LHX8	rs12041465	1:75609049	A/C	2.37E-01	intronic	2.30E-08	2.62E-05	2.60E-05	1.21E+00	2.12E-01
AC073218.1	rs892457	2:34667721	G/A	4.98E-01	intergenic	3.43E-08	3.92E-05	3.89E-05	9.38E-01	1.67E-01
14q22.1 (upstream to BMP4)	rs2357442	14:52607967	A/C	2.03E-01	intergenic	4.40E-08	5.03E-05	4.98E-05	1.11E+00	1.99E-01
PC1 (EV=1391.99)										
AGXT2	**rs37369**	**5:35037115**	**A/G**	**1.77E-01**	**missense**	**2.49E-11**	**2.85E-08**	**2.85E-08**	**-2.10E-02**	**3.08E-03**
FOXN3	**rs390345**	**14:89976534**	**A/G**	**2.47E-01**	**intronic**	**7.46E-11**	**8.55E-08**	**8.54E-08**	**-1.84E-02**	**2.77E-03**
FAM49A	rs6741412	2:16815759	G/A	3.99E-01	intronic	4.67E-10	5.35E-07	5.34E-07	-1.52E-02	2.40E-03
17q24.3	rs10512572	17:69512099	G/A	1.67E-01	intergenic	4.99E-10	5.71E-07	5.70E-07	-2.01E-02	3.17E-03
EYA1	rs79867447	8:72127562	C/T	2.19E-02	intronic	7.46E-10	8.54E-07	8.51E-07	-6.45E-02	1.03E-02
LMNA	rs12076700	1:156055099	C/G	2.28E-01	intronic	7.87E-10	9.01E-07	8.97E-07	-1.73E-02	2.76E-03
PCDH15	rs10825273	10:55968685	C/T	2.82E-01	intronic	1.04E-09	1.19E-06	1.19E-06	-1.68E-02	2.70E-03
14q22.1 (upstream to BMP4)	rs942316	14:54440983	A/C	1.21E-01	intergenic	2.66E-09	3.04E-06	3.02E-06	-2.36E-02	3.89E-03
TEX41	rs10496971	2:145769943	T/G	1.87E-01	intronic	3.71E-09	4.25E-06	4.22E-06	-1.84E-02	3.06E-03

RP11-785H20.1	rs7844723	8:122908503	C/T	4.37E-01	intergenic	8.11E-09	9.29E-06	9.21E-06	1.41E-02	2.41E-03
EYA2	rs58733120	20:45803852	G/C	2.29E-02	intronic	2.19E-08	2.51E-05	2.49E-05	-5.65E-02	9.94E-03
FAM49A	rs11096686	2:16815892	T/C	2.50E-01	intronic	2.25E-08	2.57E-05	2.55E-05	-1.65E-02	2.89E-03
EYA1	rs73684719	8:72131359	G/A	2.59E-02	intronic	2.62E-08	3.00E-05	2.96E-05	-4.94E-02	8.75E-03
XXYLT1	rs950257	3:194847650	T/A	3.87E-01	intronic	3.94E-08	4.51E-05	4.46E-05	-1.38E-02	2.48E-03

Highlighted with bold: genomic markers that reached Bonferroni corrected threshold (1.6E-07); Highlighted with blue colour: linear distances; Highlighted with red colour: craniofacial indices; Highlighted with green colour: angular distances; Highlighted with violet colour: principal component; gene/intergenic region: gene name/locus; rs#: reference SNP ID number; chromosomal location: chromosomal location of the marker based on the GRCh37/hg19; observed alleles: common alleles observed in human genome based on dbSNP build 147; MAF: minor allele frequency; genomic annotation: genomic location of the marker; UNADJ: Unadjusted p-values. BONF: Bonferroni single-step adjusted. HOLM: Holm (1979) step-down adjusted; BETA: minor allele effect size; SE: standard error.

However, given the over-conservative nature of the Bonferroni correction and also assuming that polygenic traits are likely to be dominated by numerous alleles with small causal effect we also report suggestive associations reaching the unadjusted 5.00E-08 p-value threshold (Table 1). Generally, two linear distances (nasal width and nasal tip protrusion), two angular distances (nasolabial angle and transverse nasal prominence angle), three indices (cephalic index, nasal index and nose-face width index) and one principal component revealed significant associations with 34 SNPs in 28 genes and intergenic regions (Table 1).

These factors can be arbitrarily divided into three main categories based on their cellular function: 1) genes with known roles in the craniofacial morphogenesis and/or mutated in various hereditary syndromes displaying craniofacial abnormalities; 2) genes or pseudo-genes without known function in the craniofacial morphology regulation or previously uncharacterized genes; and 3) non-protein coding genes, such as lncRNA class genes. There are also a number of significant variants that are located in the intergenic regions, with or without proximity to open reading frames (ORFs).

The majority of associated markers (n=21) are located in 17 protein-coding genes and pseudo-genes such as *AGXT2, CACNB4, COL11A1, EGFR, EYA1, EYA2, FAM49A, FOXN3, LHX8, LMNA, MYO5A, PAX3, PCDH15, RTTN, SMAD1, XXYLT1 and ZEB1*.

Five variants are present in RNA-coding (lncRNA) genes, which include *AC073218.1, RP11-494M8.4, RP11-408B11.2, RP11-785H20.1 and TEX41*.

The rest of the markers (n=6) are found in the intergenic regions, near the following genes and pseudogenes: *BMP4, HAS2-AS1, LOC124685, LOC100131241, MRPS36P3, PTCH1, SLC25A5P2, SV2B and TRNAY16P*.

Analysis of the functional annotation of significant markers revealed that one SNP represent missense mutation (rs37369), one SNP is a synonymous transversion (rs2290332), 21 markers are located in intronic sequences and 11 markers are located in intergenic regions (Table 1). The majority of significantly associated SNPs (n=27) are found in the regulatory elements of the genome, such as in transcription factor (TF) binding sites, and represent potentially functional SNPs (pfSNPs). These variants may be involved in “fine tuning” of the normal craniofacial phenotype as part of the enhancer/silencer mechanisms, as has been recently suggested [77].

The nasal area measurements, using either “n”, “prn”, “sn” or “al” landmarks, produced the majority of the total number of significant associations (6 out of 8). These measurements

include nasal width (al-al), nasal tip protrusion (sn-prn), nasolabial angle (prn-sn-ls), transverse nasal prominence angle (t_l-prn-t_r), nasal index (al-al/n-sn), and nose face width index (al-al/zy-zy). The apparent overrepresentation of associations with the nasal area may be a result of the easier allocation and consequent superior reproducibility of the nasal area landmark measurements on 3D images. It may also be the result of specific selection of candidate genes from the JAX mice database resource, which focused on mutants that displayed various nasal area abnormalities.

The analysis of direct cranial measurements and their relative indices revealed significant associations only the Cephalic index (CI) with 9 SNPs.

The association analysis of the principal components (PC) representing all the craniofacial measurements, revealed one principal component (explaining 73.3% of all the craniofacial phenotypes) that was associated with 14 genetic markers (Table 1).

In contrast to most other craniofacial association studies that focused on a specific homogeneous population group (mostly Europeans), this study included samples from several population groups, which enabled investigation of the genetic factors influencing normal craniofacial morphology in different ethnicities [71]. Self-reported ancestry however, cannot be considered fully reliable, as demonstrated previously [72, 73]. In order to address this issue we assessed the self-reported ancestry using STRUCTURE with 186 SNPs removed due to long-range disequilibrium [49]. Following the rationale that the best ancestry estimates are obtained using a large number of random markers [74], we used all the available markers (after MAF filtering) in STRUCTURE analysis. The STRUCTURE analysis resulted in clusters of 367 Europeans, 51 East Asians, 43 South Asians and 16 Africans, with 107 samples designated as admixed ancestry (Fig. 1). Of the samples tested with STRUCTURE, 459 (89%) were assigned the same ancestry cluster (sole or mixed origin) as the self-reported information. Of the remaining 57 individuals, 39 were estimated as ‘admixture’ (based on up to 20% admixture threshold) and 18 were assigned a single ancestry, different to the self-reported ancestry (Fig. 1).

The risk of detecting false positive results because of population stratification was carefully assessed and further reduced by applying an EIGENSTRAT correction. Specifically, EIGENSTRAT’s smartpca.perl was used to perform PCA-clustering in comparison to reference populations from HapMap reference clusters. The Q-Q plots of the associated traits showed the expected distribution of data after applied correction (Supplemental Figs. S1-S8).

We did not perform allele imputations on this dataset because it includes individuals from heterogenous ancestral backgrounds, with 107 subjects classified as 'admixture', based on the applied threshold of 20%. Imputation using homogenous reference populations would have introduced unnecessary bias with wrongly imputed alleles in subsequent analysis steps.

Association analyses of the non-craniofacial traits

In our attempt to identify genetic markers influencing normal variation in craniofacial traits, we incorporated 522 markers previously associated with human pigmentation traits, such as eye, skin and hair colour. These markers were included to validate the statistical methods used for the craniofacial traits association study. The association analyses of the pigmentation traits, which were based on the HWE non-filtered data, did indeed confirm previously published findings, as detailed in Table S2. It should be noted however, that these results may not necessarily confirm the validity of the craniofacial markers associations.

The application of the Hardy-Weinberg equilibrium (HWE) threshold resulted in filtering 25% of the total number of SNPs. These markers included almost all the SNPs, previously associated with pigmentation traits, such as rs12913832, rs1129038, rs8039195 and rs16891982. This is not surprising, since population-related markers are likely not being in HWE ‘a priori’. Another explanation for this observation is potential bias from partially uncorrected heterogeneous ancestry, since the ancestry correction algorithm can only minimize, rather than completely remove spurious associations [52]. In fact, the association analyses of the HWE non-filtered genotyping data with pigmentation traits (eye, skin and hair colour), demonstrated highly significant associations, concordant with the literature (Table S2).

Craniofacial gene and SNP annotations

The following section summarizes the genetic association results, providing brief annotation of the significantly associated genes and SNPs. Functional annotations, such as predicted molecular function, link to a biological process and a protein class of the 23 protein-coding genes and pseudo-genes (*AGXT2, BMP4, CACNB4, COL11A1, EGFR, EYA1, EYA2, FAM49A, FOXN3, LHX8, LMNA, MYO5A, PAX3, PCDH15, RTTN, SMAD1, XXYLT1*

414 *and ZEB1*) have been visualised using the PANTHER resource [78] and summarized in
415 supplemental materials (Supplemental Figs. S17-S19).

416 Significantly associated genes with previously demonstrated role in
417 craniofacial morphogenesis and/or mutated in hereditary syndromes
418 displaying craniofacial abnormalities

419 A potentially functional SNP rs2289266 in the intron of the Paired Box 3 gene (*PAX3*) was
420 associated with the transverse nasal prominence angle (p-value 1.95E-08). This gene is a
421 member of the paired box (*PAX*) family of transcription factors, which play critical roles
422 during foetal development. The *PAX3* protein regulates cell proliferation, migration and
423 apoptosis. Mutations in *PAX3* are associated with Waardenburg syndrome (OMIM: 193500),
424 which is characterized by a prominent and broad nasal root, a round or square nose tip,
425 hypoplastic alae, increased lower facial height and other craniofacial abnormalities.

426 Notably, three other SNPs in this gene, rs974448, rs7559271 and rs1978860, were previously
427 associated with normal variability of the nasion position [22] and the distance between the
428 eyeballs and the nasion [20]. None of these SNPs were included in this study, as a result of
429 primer design failure. No LD between rs2289266 and any of the previously associated
430 markers in the *PAX3* gene was detected. Nevertheless, the association of another variant in
431 the *PAX3* gene can be considered an independent confirmation of this gene's involvement in
432 regulation of normal craniofacial morphology.

433 SNPs rs4908280 and rs11164649 which are located in the regulatory element of the Collagen
434 gene (*COL11A1*) intronic sequence, were associated with the cephalic index (p-values 1.66E-
435 09 and 1.70E-08 respectively). *COL11A1* encodes one of the two alpha chains of type XI
436 fibrillar collagen and is known to have multiple transcripts as a result of alternative splicing.
437 The secreted protein is hypothesised to play an important role in fibrillogenesis by controlling
438 lateral growth of collagen II fibrils.

439 Notably, the same variant (rs11164649) was recently linked to normal-range effects in
440 various craniofacial traits, specifically eyes, orbits, nose tip, lips, philtrum and lateral parts of
441 the mandible, although the measurements of the cephalic index were not performed in this
442 study [93]. Our findings should be considered as independent confirmation of *COL11A2* gene
443 and its specific polymorphism rs11164649 involvement in shaping the normal craniofacial
444 morphology.

445 According to the MGI database, transgenic mice with shortened *COL11A2* mRNA (the
446 second alpha chain of type XI fibrillar collagen) display abnormal facial phenotypes,
447 including a triangular face and shorter and dimpled nasal bones [30]. Interestingly, *COL11A1*
448 and other Collagen family genes were found to be mutated in Stickler (OMIM: 604841) and
449 Marshall Syndromes (OMIM: 154780). These two inherited disorders display very similar
450 phenotypes and each is characterized by a distinctive facial appearance, with flat midface,
451 very small jaw, cleft lip/palate, large eyes, short upturned nose, eye abnormalities, round face
452 and short stature. However, the facial features of Stickler syndrome are less severe and
453 include a flat face with depressed nasal bridge and cheekbones, caused by underdeveloped
454 bones in the middle of the face. Another member of the collagen family, *COL17A1*, was
455 recently associated with the distance between the eyeballs and the nasion [23]. Our finding of
456 genetic associations of additional members of the Collagen family provides further evidence
457 of the importance of polymorphisms in these genes in determining the normal variety of
458 specific craniofacial features.

459 Intergenic SNP rs942316, which is located upstream to the Bone Morphogenetic Protein
460 (upstream to *BMP4*) gene, was strongly associated with the PC1phenotype (p-value 2.66E-
461 09). The *BMP4* gene is a transforming growth factor, belonging to the beta superfamily,
462 which includes large families of growth and differentiation factors. This gene plays an
463 important role in the onset of endochondral bone formation in humans, including induction of
464 cartilage and bone formation and specifically tooth development and limb formation. Gene
465 onthology annotations related to this gene include heparin binding and cytokine activity.
466 *BMP4* mutations have been associated with a variety of bone diseases, including orofacial
467 cleft 11 (OMIM: 600625), Fibrodysplasia Ossificans (OMIM: 135100) and microphthalmia
468 syndromic 6 (OMIM: 607932).

469 SNP rs2290332 represents a synonymous variant in the *Myosin VA* (Heavy Chain 12,
470 *Myoxin*) gene (*MYO5A*). This variant was associated with the cephalic index (p-value 5.56E-
471 10).

472 *MYO5A* is one of three myosin V heavy-chain genes, belonging to the myosin gene
473 superfamily. *Myosin V* is a class of actin-based motor proteins involved in cytoplasmic
474 vesicle transport and anchorage, spindle-pole alignment and mRNA translocation. It mediates
475 the transport of vesicles to the plasma membrane, including melanosome transport. Mutations
476 in this gene were associated with a number of neuroectodermal diseases, such as Griscelli
477 syndrome. Additional mutations in this gene were associated with a rare inherited condition

Piebaldism (OMIM:172800). The symptoms of Piebaldism include partial albinism and anomalies of the mouth area development, such as lips and philtrum abnormalities. Despite being a "silent" mutation, rs2290332 is located in the POLR2A TF binding site and may therefore affect various processes such as transcription, translation, splicing and mRNA transport, as has been shown in other studies [79].

Variant rs12041465, which is located in the intron of *LIM Homeobox 8* (*LHX8*) was associated with transverse nasal prominence angle (p-value 2.30E-08). *LHX8* is a transcription factor and a member of the *LIM homeobox* family of proteins, which are involved in patterning and differentiation of various tissue types. Mutations in this gene were associated with clefts of the secondary palate in mouse model [80, 81].

Three intronic SNPs in the Eyes Absent Homolog 1 (*EYA1*) gene were associated with several craniofacial traits. The variant rs79867447 was associated with the nose width (p-value 3.92E-08), nasal index (p-value 3.53E-08), nose-face width index (p-value 1.10E-09) and PC1 (p-value 7.46E-10). The variant rs1481800 was associated with the cephalic index (p-value 2.07E-09). The variant rs73684719 was found in association with PC1 (p-value 2.62E-08). All three variants belong to potentially regulatory elements of the genome and are likely to affect TF binding sites. No linkage disequilibrium has been detected between these markers.

The *EYA1* encoded protein functions as histone phosphatase, regulating transcription during organogenesis in kidney and various craniofacial features such as branchial arches, eye and ear. *eya1* mutated mice display various craniofacial anomalies of the inner ear, mandible, maxilla and reduced skull [30]. Mutations in the human ortholog have been associated with several craniofacial conditions such as otofaciocervical syndrome (OMIM:166780), Weyers acrofacial dysostosis (OMIM:193530) and branchiootic syndrome (OMIM:608389).

Intronic SNP rs58733120 was associated with the nose width (p-value 5.37E-10), nasal index (p-value 9.46E-09), nose-face width index (p-value 3.38E-09) and PC1 (p-value 2.19E-08) phenotypes. This variant is located in the regulatory element of the *EYA2* gene, which belongs to the same eyes absent protein family as *EYA1* and plays a similar role in the embryonic development. An orthologue *eya2* gene encodes a transcriptional activator in mice and may play a role in eye development. Both *EYA1* and *EYA2* genes were shown to be expressed in the ninth week of human embryonic development [82]. None of the human craniofacial disorders were associated with *EYA2* gene to date.

SNP rs12076700 in the intron of the *Lamin A* gene (*LMNA*) was associated with the transverse nasal prominence angle (1.54E-09) and PC1 (p-value 7.87E-10).

*LMNA***,** together with other *Lamin* proteins, is a component of a fibrous layer on the nucleoplasmic side of the inner nuclear membrane, which provides a framework for the nuclear envelope and also interacts with chromatin. *LMNA* encoded protein acts to disrupt mitosis and induces DNA damage in vascular smooth muscle cells, leading to mitotic failure, genomic instability, and premature senescence of the cell. This gene has been found mutated in Mandibuloacral Dysplasia which is characterized by various skeletal and craniofacial abnormalities, including delayed closure of the cranial sutures and undersized jaw [83].

Variant rs74884233 was associated with the transverse nasal prominence angle (p-value 1.20E-08). This variant is located in the intron of the *Rotatin* gene (*RTTN*). *RTTN* gene is involved in the maintenance of normal ciliary structure, which in turn effects the developmental process of left-right organ specification, axial rotation, and perhaps notochord development.

SNP rs17020235 was associated with the nasolabial angle (p-value 2.07E-09). This potentially functional variant is located in the intron of the *SMAD* Family Member 1 gene (*SMAD1*). *SMAD1* is a transcriptional modulator activated by BMP (bone morphogenetic proteins) type 1 receptor kinase, which is involved in a range of biological activities including cell growth, apoptosis, morphogenesis, development and immune responses.

SMAD1 mutant mice display anterior truncation of the head with only one brachial arch present. In human, *SMAD1* mutations (together with *RUNX2*), are associated with the Cleidocranial Dysplasia (OMIM:119600), which is a Craniosynostosis-type disorder affecting cranial bones, palate and other tissues.

SNP rs950257 was associated with the PC1 trait (p-value 3.94E-08). This intronic variant is located in the *XXYLT1* gene, which codes for Xyloside Xylosyltransferase 1. This protein is an Alpha-1,3-xylosyltransferase, which elongates the O-linked xylose-glucose disaccharide attached to *EGF*-like repeats in the extracellular domain of Notch proteins signalling network. Notch proteins are the key regulators of embryonic development, which demonstrate a highly conserved sequence in various species. Interestingly, mutations in Notch proteins are associated with Hajdu–Cheney syndrome (OMIM:10250) and Alagille syndrome (OMIM:118450). The main phenotypic symptoms of these conditions include

various malformations of the craniofacial tissues, including broad, prominent forehead, deep-set eyes and a small pointed chin.

SNP rs17335905 was associated with the nose-face width index (p-value 4.74E-08). This potentially functional variant is located in the intron of the *EGFR* gene, which encodes the Epidermal Growth Factor Receptor. *EGFR* is a cell surface protein that binds to epidermal growth factor (*EGF*). Binding of the protein to a ligand induces activation of several signalling cascades and leads to cell proliferation, cytoskeletal rearrangement and anti-apoptosis. Mouse carrying mutations in *EGFR*, express short mandible and cleft palate.

Significantly associated SNPs, located in genes or pseudo-genes that were not linked to craniofacial morphology regulation or genes with unknown function

Intronic variant rs59037879 in the Zinc Finger E-Box Binding Homeobox 1 (*ZEB1*) was found associated with cephalic index (p-value 6.27E-10), and transverse nasal prominence angle (p-value 5.31E-12). This gene encodes a zinc finger transcription factor, which is a transcriptional repressor. It regulates expression of different genes, such as interleukin-2 (*IL-2*) gene, ATPase transporting polypeptide (*ATP1A1*) gene and E-cadherin (*CDH1*) promoter in various cell types and also represses stemness-inhibiting microRNA. Mutations in this gene were previously associated with Corneal Dystrophy and various types of cancer.

A missense mutation rs37369 in the Alanine--Glyoxylate Aminotransferase 2 gene (*AGXT2*) was associated with nose width (p-value 1.04E-09), nasal index: (p-value 1.25E-10), transverse nasal prominence angle (p-value 1.46E-09) and PC1 (p-value 2.49E-11). This protein plays an important role in regulating blood pressure in the kidney through metabolizing asymmetric dimethylarginine (*ADMA*), which is an inhibitor of nitric-oxide (NO) synthase.

An intronic SNPs rs16830498, located in the regulatory element of the Calcium Channel Voltage-Dependent Beta 4 Subunit (*CACNB4*) gene intron, were significantly associated with cephalic index (p-value 7.57E-11).

The beta subunit of voltage-dependent calcium channels may increase peak calcium current by shifting the voltage dependencies of activation and inactivation, modulating G protein

inhibition and controlling the alpha-1 subunit membrane targeting. *CACNB4* may be expressed in different isoforms through alternative splicing. Certain mutations in this gene have been associated with various forms of epilepsy, although no association with normal or abnormal craniofacial variation has been previously reported.

Potentially functional intronic SNP rs10825273 located in the regulatory elements of the Protocadherin-Related 15 (*PCDH15*) gene, was found in association with cephalic index (p-value 9.93E-09) and PC1 (p-value 1.04E-09). *PCDH15* is a member of the cadherin superfamily, which encodes an integral membrane protein that mediates calcium-dependent cell-cell adhesion and is known to have numerous alternative splicing variants. It plays an essential role in the maintenance of normal retinal and cochlear function. Mutations in this gene result in hearing loss and are associated with Usher Syndrome Type IIA (OMIM: 276901).

Two intronic variants in the Family With Sequence Similarity 49 Member A gene (*FAM49A*) were associated with multiple craniofacial traits. rs6741412 was found in association with the transverse nasal prominence angle (p-value 2.75E-09) and PC1 (p-value 4.67E-10). rs11096686 was associated with PC1 (p-value 2.25E-08). The *FAM49A* protein is known to interact with hundreds of miRNA molecules during pre-implantation of the mouse embryo and also expressed in the developing chick wing, but no information on its specific function or disease association have been identified.

SNP rs390345, located in the intronic regulatory sequence of the Forkhead Box N3 gene (*FOXN3*), was associated with the PC1 (p-value 7.46E-11). *FOXN3* encodes multiple splicing variants and acts as a transcriptional repressor. It is proposed to be involved in DNA damage-inducible cell cycle arrests at G1 and G2. There are no previous reports on *FOXN3* association with either normal craniofacial development or pathological conditions.

Significantly associated SNPs located in the non-protein coding genes, such as lncRNA class genes

Intronic SNP rs10496971 in the *TEX41* (Testis Expressed 41) gene produced significant associations with transverse nasal prominence angle (p-value 5.52E-09), cephalic index (p-value 5.315E-09) and PC1 (p-value 3.71E-09).

TEX41 is a long intergenic non-protein coding RNA (lncRNA) class gene, which is located on chromosome 2 and has 43 transcript variants as a result of alternative splicing. lncRNAs are known as regulators of diverse cellular processes. However, the function of this gene remains unknown. Despite its name, this gene is expressed in a variety of tissues, with the highest demonstrated levels in kidney. Its potential involvement in craniofacial genetics, and specifically in influencing normal facial variation, has not been reported previously. Notably, the rs10496971 variant is located in the regulatory element of the genome (as well as 49 other associated SNPs) and may influence normal craniofacial morphology by affecting either enhancer or silencer sequences or transcriptional factor (TF) binding sites [77].

The SNP rs1482795, located in the RNA gene *RP11-494M8.4*, was associated with the nose width (p-value 7.68E-10) and nasal index (p-value 1.83E-08) measurements.

Both SNPs rs892457 and rs892458 located in the non-protein coding lncRNA gene *AC073218*.1, were associated with the transverse nasal prominence angle (p-value 3.43E-08) and (p-value 1.73E-08), respectively.

SNP rs7311798, located in the lncRNA gene *RP11-408B11.2* was associated with the nasal index (p-value 1.77E-08).

SNP rs7844723 in the *RP11-785H20.1* (lncRNA gene) was associated with the PC1 (p-value 8.11E-09) phenotype.

SNP rs2357442 was associated with the transverse nasal prominence angle (p-value 4.40E-08). This variant is located in the Long Interspersed Nuclear Element 1 (*LINE-1*) retrotransposon sequence, which in turn shows homology with uncategorized mRNA KC832805 on the Y-chromosome.

LINE-1 elements comprise approximately 21% of the human genome, and have been shown to modulate expression and produce novel splice isoforms of transcripts from genes that span or neighbour the LINE-1 insertion site. In addition, rs2357442 is located close to three pseudo-genes with unknown function: *SLC25A5P2, LOC100130842* and *RP11-1033H12.1,* while the last two represent RNA-coding lncRNA genes.

Significantly associated SNPs located in the intergenic regions

SNP rs10512572, located between *Serpine1 MRNA Binding Protein 1* pseudogene (*LOC100131241*) and *MyosinLight Chain 6 Alkali Smooth Muscle and Non-Muscle* pseudogene (*LOC124685*), was associated with nasal tip protrusion (p-value 2.22E-08),

transverse nasal prominence angle (p-value 1.38E-11) and PC1 (p-value 4.99E-10). While pseudogenes in general are non-protein coding, their sequences can be functional and play important roles in different biological processes [85]. It should be noted that some genes may be incorrectly defined as pseudogenes, based solely on their sequence computational analysis [86]. The function of these two pseudogene sequences is unknown.

SNP rs8035124 was significantly associated with the nose width (p-value 1.52E-10). This variant is located between the Synaptic Vesicle Glycoprotein 2B (*SV2B*) and Transfer RNA Tyrosine 16 (Anticodon GUA) Pseudogene (*TRNAY16P*) genes. The *SV2B* is a protein coding gene, which plays a role in the control of regulated secretion in neural and endocrine cells. The *TRNAY16P* is a pseudogene with unknown function.

Additional SNP rs373272 was associated with cephalic index (p-value 2.40E-08). However, no genes were identified within 50 kb window of its chromosomal location.

Discussion

This study focused on the identification of genetic markers in a set of candidate genes associated with various craniofacial traits, representing the most comprehensive scan for genetic markers involved in normal craniofacial development performed to date. We identified 8 craniofacial significantly associated (unadjusted p-value < 5.00E-08) with 34 genomic variants in 28 genes and intergenic regions. Following the application of Bonferroni correction (adjusted p-value threshold of 1.6E-07), associations were observed between 5 craniofacial traits (nasal width, cephalic index, nasal index, transverse nasal prominence angle and principal component) and 6 SNPs (rs8035124, rs16830498, rs37369, rs59037879, rs10512572 and rs390345) located in 6 genes and intergenic regions (15q26.1, 17q24.3, *CACNB4, AGXT2, ZEB1 and FOXN3* respectively). We report all the significant markers that met the less stringent GWAS threshold (p-value<5.00E-08), as Bonferroni correction is generally considered over-conservative, especially when analysing complex traits such as craniofacial morphology, which is likely to be influenced by a large number of alleles with relatively small individual effect, similar to height [89, 90].

The association of the *PAX3* gene and the *COL11A1* gene with transverse nasal prominence angle and cephalic index respectively, confirms previous findings [11, 22, 23, 91]. In fact, an intronic SNP rs11164649 that was associated with cephalic index in the current study, was

recently associated with normal-range effects in various craniofacial traits and used for their prediction [91], while the other variants in *COL11A1* (rs4908280) and in *PAX3* (rs2289266) have not been reported previously. The rest of the identified associations are also novel. These include 21 significantly associated markers in protein-coding genes and pseudo-genes, such as *AGXT2, CACNB4, EGFR, EYA1, EYA2, FAM49A, FOXN3, LHX8, LMNA, MYO5A, PCDH15, RTTN, SMAD1, TEX41, XXYLT1 and ZEB1*. Additional 7 significantly–associated SNPs are found in intergenic regions adjacent to several loci, such as *BMP4, LOC124685, LOC100131241 and PTCH1*. Some of these genes were previously linked to craniofacial embryogenesis, while others represent novel associations.

Six genetic variants were found in lncRNA genes, which have not been previously linked to craniofacial morphogenesis before. These findings may suggest there may be a yet unexplored level of epigenetic regulation affecting craniofacial morphology. lncRNAs are a recently discovered class of factors, whose expression is thought to be important for the regulation of gene expression through several different mechanisms involving competition with transcription by recruitment of specific epigenetic factors to promoter regions, as well as indirectly affecting gene expression by interacting with miRNA and other cellular factors [92]. The comprehensive role of epigenetic regulation in general, and in craniofacial embryonic development in particular, is poorly understood. There is a limited number of recent studies revealing thousands of enhancer sequences, predicted to be active in the developing craniofacial complex in mice [77, 93] and potentially in humans. Both the epistatic and epigenetic interactions may represent a more complex level of craniofacial morphology regulation and require further investigation.

Even though a relatively high number of phenotypes were studied (92 linear and angular measurements and indices), this may still represent an oversimplification of the complexity of the human face. Despite the importance of the association between specific 3D measurements and SNPs demonstrated in this study, the association of facial shapes, represented by the principal components should better represent the face. Given that embryonic developmental processes such as cell proliferation, polarity orientation and migration occur in a 3D environment, principal components that in essence denote specific facial shapes, may provide a more accurate representation of these processes. However, only one of the 10 principle components showed significant associations at the GWAS threshold level. While the explanation of this observation is unclear, it is consistent with other similar studies [22, 23]. The specific anthropometric measurements on the other hand, produced numerous significant

696 associations, identifying many genes and intergenic regions that appear to play important
697 roles in the development of normal human facial appearance. The major limitation of this
698 study is the replication of these results that has not been performed yet due to time and
699 budget constraints. However, the confirmation of the two previously associated genes (*PAX3*
700 and *COL11A1*) supports the validity of our findings.

701 Given the high complexity of the face, as well as the composite nature of the genetic
702 regulation that affects its development, alternative comprehensive approaches of capturing
703 facial morphology would be beneficial. A number of such methods has recently revealed
704 additional genes with specific polymorphisms associated with the development of
705 craniofacial traits within the normal variation range [91, 94]. Further studies may involve the
706 use of these or alternative methods to capture the majority of variation in craniofacial traits.
707 Craniofacial phenotypes, together with additional external visible traits such as sex, age and
708 BMI and ancestry, could be treated as a "vector", which could then be used to predict
709 appearance [95].

710 A recent attempt to predict facial appearance was performed using only 24 SNPs [96]. This
711 approach has promise, although it is largely based on reconstruction of a 'facial composite
712 image' through prediction of ancestry, sex, pigmentation and human perception of faces. This
713 approach is reasonable, but it does not negate the use of association studies looking at
714 specific craniofacial traits. Genetic association studies of a large scope of individual
715 anthropometric measurements are essential to provide information on specific genes and their
716 polymorphisms, which affect these traits and may therefore be useful in predicting the size
717 and the shape of specific facial features.

718 Additional association studies on large sample sizes, incorporating dense SNP panels or
719 whole genome sequencing approaches, in conjunction with either a comprehensive set of
720 anthropometrical measurements or morphologically adequate representation of the
721 craniofacial characteristics would be a valuable adjunct to the promising results obtained in
722 this study. These studies will not only improve our understanding of the genetic factors
723 regulating craniofacial morphology, but will also enable a better prediction of the visual
724 appearance of a person from DNA.

725

Methods

Sample collection and ethics statement

A total of 623 unrelated individuals, mostly Bond University (Gold Coast, Australia) students, of Australian ancestry were recruited. The participants provided their written informed consent to participate in this study, which was approved by the Bond University Ethics committee (RO-510). To minimize any age-related influences on facial morphology the samples were largely collected from volunteers aged between 18 and 40. The mean age of the volunteers was 26.6 (SD ± 8.9). Following the exclusion of the individuals who had experienced severe facial injury and/or undergone facial surgery (e.g. nose or chin plastics) 587 samples remained for the further step of DNA sequencing.

Each participant donated four buccal swabs (Isohelix, Cell Projects, Kent, UK). 3-Dimentional (3-D) facial scans and three direct cranial measurements were obtained as described below. Samples with low DNA quantity or low quality facial scans were eliminated leaving 587 DNA samples for subsequent genotyping.

Additional phenotypic trait information such as height, weight, age, sex, self-reported ancestry (based on the grandparents from both sides), eye lid (single or double), ear lobe (attached or detached), hair texture (straight, wavy, curly or very curly), freckling (none, light, medium or extensive), moles (none, few or many), as well as eye skin, and hair pigmentation was collected by a single examiner in order to reduce potential variation. The pigmentation traits were arbitrary assigned according to previously published colour charts [26-28].

3D images collection and analysis

Craniofacial scans were obtained using the Vivid 910 3-D digitiser (Konica Minolta, Australia) equipped with a medium range lens with a focal length of 14.5 mm. The scanner output images were of 640 x 480 pixels resolution for 3D and RGB data. Two daylight fluorescent sources (3400K/5400K colour temperature) were mounted at approximately 1.2 meters from the subject's head to produce ambient light conditions.

The scanner was mounted approximately one meter from the volunteer's head. Each volunteer remained in an upright seated position and kept a neutral facial expression during the scan. Subjects with long hair pulled their hair behind the ears or were asked to wear a hair net. Glasses and earrings were removed.

Each volunteer was scanned from a distance of approximately one meter from three different angles (front and two sides). The final merged 3D image was produced by semi-automatically aligning the three scans and manually cropping non-overlapping or superfluous data such as the neck area and hair using Polygone® software (Qubic, Australia). The complete coordinates of each merged 3D image were then saved in a 'vivid' file format (vvd) and exported to Geomagic® software (Qubic, Australia) for subsequent image processing.

Based on the anthropometrical literature [29] 32 anthropometrical landmarks were manually identified on each 3-D image using the Geomagic software (Fig. 2 and Supplemental Table S1). Each landmark was represented by 'x', 'y' and 'z' coordinates as part of the Cartesian coordinate system. The coordinates were exported to an Excel spreadsheet for subsequent calculation of 86 Euclidean distances, including 54 linear distances, 10 angular distances and 21 indices (ratios) between the linear distances (Fig. 2 and Table 2).

Additionally, three direct cranial measurements: maximum cranial breadth (Euryon – Euryon), maximum cranial length (Gonion – Opisthocranium) and maximum cranial height (Vertex – Gnathion), were collected manually using a digital spreading calliper (Paleo-Tech Concepts, USA). Based on the craniofacial and body height measurements, three craniofacial ratios were calculated: Cephalic index: (eu-eu)/(g-op), Head width – Craniofacial height index: (eu-eu)/(v-gn) and Head – Body height index: (v-gn)/(body height), as summarised in Table 2.

Table 2. Craniofacial anthropometric measurements recorded in the study and used for genetic association analyses.

Manual craniofacial measurements
• V-Gn (Maximum Craniofacial height) • Eu-Eu (Maximum Head Width) • G-Op (Maximum Head Length)

- Cephalic index: (eu-eu)/(g-op)
- Head width – Craniofacial height index: (eu-eu)/(v-gn)
- Head – Body height index: (v-gn)/(body height)

3D facial measurements

Linear facial distances

- Total face height: tr-gn
- Face width: zy-zy
- Morphological face height: n-gn
- Physiognomical face height: n-sto
- Lower profile height: prn-gn
- Lower face height: sn-gn
- Lower third face depth: t(l)-gn
- Middle face depth: t(l)-prn
- Middle face height (right): go(r)-zy(r)
- Middle face height (left): go(l)-zy(l)
- Middle face width 1: t(r)-t(l)
- Middle face width 2 (left): zy(l)-al(l)
- Middle face width 2 (right): zy(r)-al(r)
- Upper face depth: (left): t(l)-tr
- Upper face depth: (right): t(r)-tr
- Upper third face depth: t(l)-n
- Forehead height: g-tr
- Extended forehead height: tr-n
- Glabella –Gnathion distance: g-gn
- Supraorbital depth: t(l)-g
- Trichion – Zygion distance (left): tr-zy(l)
- Trichion – Zygion distance (right): tr-zy(r)
- Nasion - Zygion distance (left): n-zy(l)
- Nasion - Zygion distance (right): n-zy(r)
- Zygion – Gnathion distance (left): zy(l)-gn
- Zygion – Gnathion distance (right): zy(r)-gn
- Interendocanthal width: en-en
- Interexocanthal width: ex-ex
- Eye fissure width (left): en(l)-ex(l)
- Eye fissure width (right): en(r)-ex(r)
- Eye fissure height (left): ps(l)-pi(l)
- Eye fissure height (right): ps(r)-pi(r)
- Ear height (left): sa(l)-sba(l)
- Ear width (left): t(l)-pa(l)
- Nasal bridge length: n-prn
- Nose height: n-sn
- Nose width: al-al
- Nasal tip protrusion: sn-prn

- Ala length (left): prn-al(l)
- Ala length (right): prn-al(r)
- Gonion - Trichion distance (left): go(l)-tr
- Gonion - Trichion distance (right): go(r)-tr
- Gonion – Glabella distance: g-pg
- Pronasale - Gonion distance (left): prn-go(l)
- Pronasale - Gonion distance (right): prn-go(r)
- Chin height: sl-gn
- Mandibular region depth (right): t(r)-gn
- Mandible width: go-go
- Mandible height: sto-gn
- Lower jaw depth (left): gn-go(l)
- Lower jaw depth (right): gn-go(r)
- Mouth width: ch-ch
- Upper vermilion height: ls-sto
- Lower vermilion height: li-sto

Angular facial distances

- Nasal tip angle: (n-prn-sn)
- Nasal vertical prominence angle: (tr-prn-gn)
- Transverse nasal prominence angle 1: (zy(l)-prn-zy(r))
- Transverse nasal prominence angle 2: (t(l)-prn-t(r))
- Nasolabial angle: (prn-sn-ls)
- Nasofrontal angle: (g-n-prn)
- Nasion depth angle: (zy(l)-n-zy(r))
- Nasomental angle: (n-prn-pg)
- Forehead nasal angle: (tr-n-prn)
- Chin prominence angle: (go(l)-gn-go(r))

Ratios (indices)

- Forehead height ratio: (tr-n)/(go(r)-go(l))
- Upper face height ratio: (n-sn)/(go(r)-go(l))
- Lower face height ratio: (sn-gnx)/(go-go)
- Anterior face height 1 ratio: (n-gn)/(go-go)
- Anterior face height 2 ratio: (n-gn)/(zy-zy)
- Face height index: (n-gn)/(tr-gn)
- Upper – Lower face ratio: (tr-g)/(sn-gn)
- Upper face height ratio: (n-sn)/(sn-gn)
- Upper face width ratio: (n-sn)/(zy-zy)
- Total anterior face height ratio: (tr-gn)/(zy-zy)
- Mouth width ratio: (ch-ch)x100/(en-en)
- Mandible – Face width ratio: (go-go)/(zy-zy)
- Mandible index: (sto-gn)x100/(go-go)
- Mandible – Interexocanthion distance ratio (go-go)/(ex-ex)

- Interendocanthion distance ratio: (en-en)/(al-al)
- Intercanthal index: (en(r)-en(L)/(ex(r)-ex(l)
- Intercanthal – Intracanthal index: (ex(r)-en(r)/(en(l)-ex(l)
- Nasal index: (al-al)x100/(n-sn)
- Nose-face height index: (n-sn) /(n-gn)
- Nose-face width index: (al-al)/(zy-zy)
- Nasal tip protrusion – nose width index: (sn-prn)/(al-al)
- Nasal tip protrusion –Nose height index: (sn-prn)/(n-sn)

Phenotypic traits summary

A total of 54 linear distances, 10 angular distances and 21 indices (ratios) between the linear distances were calculated based on the Cartesian coordinates of 32 anthropometric landmarks that were manually mapped on each of the 587 3-D facial images (Fig. 2, Fig. 3, Table 2 and Supplemental Table S1). Three additional craniofacial distances were obtained by direct measurement of subjects' heads and used to calculate three indices: maximum cranial breadth, maximum cranial length and maximum cranial height, cephalic index, head width – craniofacial height index and head – body height index (Table 2). Information on the eyelid and earlobe morphology (single/double and attached/detached respectively) was recorded. Furthermore, the linear and angular facial distances were used to calculate 10 principal components (PCs). Additional phenotypic traits such as eye, skin and hair pigmentation, hair texture, freckling, moles, height, weight, BMI, age and sex were collected. In total, the data on 104 craniofacial phenotypic traits were recorded and used for genetic association analyses.

The phenotypic data collection by a single examiner achieved more consistent measurements from the 3-D image analyses. In addition, all measurements were based on the images of participants within a narrow age range 26.6 (SD ± 8.9).

DNA extraction and quantification

DNA was purified from buccal swabs using the Isohelix DDK isolation kit (Cell Projects, Kent, UK) according to the manufacturer instructions. DNA samples were quantified using a Real Time quantitative PCR (q-PCR) method using a Bio-Rad CFX96 (Bio-Rad, Gladesville,

Australia). This assay amplified a 63bp region of the OCA locus. The primer sequences were 5'-GCTGCAGGAGTCAGAAGGTT-3' (forward primer) and 5'-CATTTGGCGAGCAGAATCC-3' (reverse primer) at a final concentration of 200mM. All DNA samples were additionally quantified using the Qubit 2.0 fluorimeter (Invitrogen) prior to library construction as per manufacturer recommendations.

Candidate genes and SNPs selection

Two main complementary strategies were used to generate a preliminary list of candidate genes and genetic markers. The first focused on searching the literature and web resources for candidate genes involved either in normal craniofacial variation or in craniofacial malformations in humans and model organisms (Supplemental Table S2).

The search for candidate genes focused not only on specifically defined craniofacial disorders, but also on genetic syndromes with various manifestations of craniofacial malformations, such as Down syndrome, Noonan Syndrome, Floating-Harbor Syndrome and others, as detailed in Supplemental Table S2. The main resources for locating candidate genes in the animal models were Mouse Genome Informatics [30] and AmiGo tool [31] The main resources for identifying candidate genes in the human genome were OMIM [32] and GeneCards [33]. A comprehensive list of web resources used for candidate gene search is detailed in the Supplemental Appendix S1.

The second approach initially implemented a broad search for high Fst SNPs, such as ancestry informative markers (AIMs), with the rationale that many genes affecting craniofacial traits would have significantly different allele frequencies across populations. AIMs were selected from a variety of published and online resources [34-43].

The relevant genes obtained by both approaches were subsequently checked for potential involvement in craniofacial embryogenesis, limb development and bilateral body symmetry. It should be noted however, that the final candidate gene list was not limited to craniofacial genes and included high Fst SNPs in genes with unknown function as well as markers located in intergenic regions, potentially possessing regulatory functions.

The resulting set of SNPs was further screened for high Fst SNPs (≥0.45) in three '1000 genomes' populations (CAU, ASW, CHB) using ENGINES browser [44] as well as potentially functional polymorphisms, such as non-synonymous SNPs [45], markers in

838 transcription factor binding sites [46] and splicing sites [47] using various web resources, as
839 detailed in Supplemental Appendix S1 and reviewed on the GenEpi website [48]. The
840 candidate markers search resulted in identification of 1,319 SNPs, located in approximately
841 177 genes/intergenic regions, as discussed in the Results section.

842 The chromosomal locations of final candidate markers were submitted to the custom
843 Ampliseq primer design pipeline (Life Technologies), according to manufacturer
844 recommendations. There were primer design difficulties for 881 markers. The marker list was
845 therefore redesigned to include alternative tagging markers showing high linkage
846 disequilibrium with the markers that failed initial primer design, resulting in 1,670 candidate
847 genetic markers. Inclusion of SNPs with MAF<1% added additional 4,381 genetic markers
848 (6,051 in total). The final custom Ampliseq panel was manufactured as two separate pools of
849 849 and 847 primer pairs, with each amplicon covering between 125 bp and 225 bp, therefore
850 possibly containing more than one polymorphism, and in total covering 15.78 kb of the
851 reference human genome. This panel included 1,319 initially targeted craniofacial and
852 pigmentation candidate markers as well as 4,732 markers in LD with original candidate SNPs
853 that failed primer design.

854 Inclusion of novel, rare SNPs (MAF<1%) increased the final number of genotyped markers
855 to 8,518 SNP in all sequenced DNA samples, although the markers with MAF≤2% were not
856 included in the association study. The list of all genotyped markers and their respective genes
857 is detailed in Table S1.

858 SNP genotyping and data analysis

859 Multiple DNA libraries were constructed from sets of 32 Ion Xpress™ (Life
860 Technologies) barcoded samples using the Ion AmpliSeq™ library Kit 2.0 (Life
861 Technologies) in conjunction with two custom primer mixes that were pooled according to
862 manufacturer recommendations. Libraries were quantified using the Ion Library Quantitation
863 kit (Life Technologies) and pooled in equal amounts for emulsion PCR, which was
864 performed using the OneTouch™ 2 instrument (Life Technologies) according to
865 manufacturer recommendations. 587 DNA samples were genotyped by massively parallel
866 sequencing on the Personal Genome Machine (PGM) (Life Technologies) using the
867 Sequencing 200 v2 kit and 316 Ion chips (Life Technologies).

868 Raw sequencing data were collected and processed on the Torrent Suite Server v3.6.2 using
869 default settings. Alignment and variant calling were performed against the human genome

reference (hg19) sequence at low stringency settings. Binary alignment map (BAM) files were generated and exported to the Ion Reporter™ (IR) cloud-based software for SNP annotation against the reference hotspot file. The IR analysis resulted in generation of the individual variant caller files (VCF) with genotype calls for each sample as well as various statistics of the sequencing quality.

To reduce potential bias of the self-reported ancestry, ancestry inferences were obtained by 3,302 markers using STRUCTURE version 2.3.4 with default parameters as per software developer recommendations [49]. SNPs in long-range Linkage Disequilibrium (> 100,000 bp) were excluded from the STRUCTURE run. The ancestry was estimated based on four predefined population clusters: Europeans, East Asians, South Asians and Africans, according to software developer recommendations. Relative allele calls for four predefined HapMap population clusters (CEU, YRI, CHB and JPT) were used as reference populations [50]. The ancestry origin was estimated as a single (unmixed) source where the main ancestry cluster could be affiliated with at least 80% of the total mixed ancestry. The samples with mixed ancestry (>20% admixture) were assigned to an 'Admixture' cluster.

Association analyses were performed using SNP & Variation Suite v7 (SVS) (Golden Helix, Inc., Bozeman, MT) and replicated using PLINK v1.07 software [51]. Statistical analyses in both software programs were performed using linear regression with quantitative phenotypes, and logistic regressions with binary phenotypes under the assumption of an additive genetic model, while each genotype was numerically encoded as 0, 1 or 2. Population stratification correction, incorporated by EIGENSTRAT program was implemented in the analyses [52, 53]. In order to reduce any potential confounding effects, all the craniofacial traits association analyses were performed using sex, BMI and EIGENSTRAT ancestry clusters as covariates. In PLINK, p-values were adjusted using the '–adjust' option. The final reported association results are based on the PLINK statistical analyses with the EIGENSTRAT PCA clusters, BMI and gender as covariates.

Annotation analysis of the significantly associated genes was performed using the GeneCards, ENTREZ and UniProtKB web portals [33, 54]. The MalaCards web site was used to detect association between the genes and hereditary syndromes [55]. The GeneMania web site was used to identify a functional network among the genes and encoded proteins [56]. Gene ontology web resource was used to find orthologs of human genes in other organisms [31, 57]. The MGI database was used to search for the phenotype in relevant

902 craniofacial mouse gene mutants [30]. The dbSNP, 1000 genomes, SNPnexus and Alfred
903 websites were used for SNP annotations [58-61].

904 The SNP Annotation and Proxy Search (SNAP) web portal was used to find SNPs in linkage
905 disequilibrium (LD) and generate LD plots, based on the CEU population panel from the
906 1000 genomes data set, within a distance of up to 500kb and an r^2 threshold of 0.8 [62].

907 The Regulome database and potentially functional database (PFS) searches were
908 implemented to annotate SNPs with known and predicted regulatory elements in the
909 intergenic regions of the *H. sapiens* genome [47, 63].

910

911 List of abbreviations

912 3D: 3-Dimentional; AIMs: ancestry informative markers; ASW: African ancestry in
913 Southwest USA; BAM: Binary alignment map; BMI: Body Mass Index; CAU: Caucasian;
914 CHB: Han Chinese in Beijing, China; ENGINES: ENtire Genome INterface for Exploring
915 Snps; EVT: Externally visible characteristic; DVI: Disaster victim identification; FDP:
916 Forensic DNA phenotyping; GWAS: Genome wide association studies; HWE: Hardy-
917 Weinberg equilibrium; JPT: Japanese in Tokyo, Japan; LD: linkage disequilibrium;
918 lncRNAs: long non-coding RNAs; LINE-1: Long Interspersed Nuclear Element 1; MAF:
919 Minor allele frequency; measurement error; ME: Measurement error; MD: Mean difference;
920 OMIM: Online Mendelian Inheritance in Man; ORFs: open reading frames; pfSNP:
921 Potentially functional SNP; PCA: Principal component analysis; RGB: Red, Green, Blue
922 (colours); SNP: Single-nucleotide polymorphism; SNAP: SNP Annotation and Proxy Search;
923 STR: Short tandem repeat; TF: Transcription factor; VCF: Variant Call Format; YRI: Yoruba
924 in Ibadan, Nigeria.

925

926 Declarations

927

928 Ethics and consent to participate

929 The participants provided their written informed consent to participate in this study, which
930 was approved by the Bond University Ethics committee (RO-510).

Competing interests

The authors declare that they have no competing interests.

Authors' contributions

MB designed the study, carried out the molecular genetic studies, carried out the data analysis, participated in the statistical analysis and drafted the manuscript. PB performed the statistical analysis and drafted the manuscript. AvD participated in the design of the study and drafted the manuscript. All authors read and approved the final manuscript.

Consent to Publish

Not applicable

Availability of data and materials

The genomic data supporting the conclusions of this article are included within the article and its additional files.

Funding

The funding for this research was provided by the Technical Support Working Group (Award Number: IS-FB-2946) and Pelerman Holdings Pt Ltd.

Acknowledgments

We would like to thank the volunteers who participated in this study without whom we could not have performed this research. We would like to thank Olga Kondrashova who helped

with the sample collection. We also thank Technical Support Working Group (TSWG) and Pelerman Holdings Pt Ltd for their generous support of this project.

References

1. Kohn LAP. The Role of Genetics in Craniofacial Morphology and Growth. Annual Review of Anthropology. 1991;20:261-78. doi: 10.2307/2155802.

2. Sperber GH, Sperber SM, Guttmann GD. Craniofacial embryogenetics and development. 2nd ed. Shelton, CT: People's Medical Pub. House USA; 2010. 250p. ill. (some colour) p.

3. Richtsmeier JT, Cheverud JM. Finite element scaling analysis of human craniofacial growth. Journal of craniofacial genetics and developmental biology. 1986;6(3):289-323. PubMed PMID: 3771738.

4. Neubauer S, Gunz P, Hublin JJ. The pattern of endocranial ontogenetic shape changes in humans. J Anat. 2009;215(3):240-55. doi: 10.1111/j.1469-7580.2009.01106.x. PubMed PMID: 19531085; PubMed Central PMCID: PMC2750758.

5. Sturm RA. Molecular genetics of human pigmentation diversity. Human Molecular Genetics. 2009;18(R1):R9-R17. doi: 10.1093/hmg/ddp003.

6. Shkoukani MA, Chen M, Vong A. Cleft Lip - A Comprehensive Review. Front Pediatr. 2013;1:53. doi: 10.3389/fped.2013.00053. PubMed PMID: 24400297; PubMed Central PMCID: PMC3873527.

7. Kimonis V, Gold J-A, Hoffman TL, Panchal J, Boyadjiev SA. Genetics of Craniosynostosis. Semin Pediatr Neurol. 2007;14:150-61.

8. Weinberg SM, Naidoo SD, Bardi KM, Brandon CA, Neiswanger K, Resick JM, et al. Face shape of unaffected parents with cleft affected offspring: combining three-dimensional surface imaging and geometric morphometrics. Orthodontics & Craniofacial Research. 2009;12(4):271-81. doi: 10.1111/j.1601-6343.2009.01462.x.

9. Anna K Coussens CRW, Ian P Hughes, C, Phillip Morris, Angela van Daal, Peter J Anderson, Barry C Powell. Unravelling the molecular control of calvarial suture fusion in children with craniosynostosis. BMC Genomics. 2007;8:458.

10. Coussens AK, Hughes IP, Wilkinson CR, Morris CP, Anderson PJ, Powell BC, et al. Identification of genes differentially expressed by prematurely fused human sutures using a

984 novel in vivo[thin space]-[thin space]in vitro approach. Differentiation. 2008;76(5):531-45.
985 doi: DOI: 10.1111/j.1432-0436.2007.00244.x.
986 11. Boehringer S, van der Lijn F, Liu F, Gunther M, Sinigerova S, Nowak S, et al.
987 Genetic determination of human facial morphology: links between cleft-lips and normal
988 variation. Eur J Hum Genet. 2011;19(11):1192-7. doi: 10.1038/ejhg.2011.110. PubMed
989 PMID: 21694738; PubMed Central PMCID: PMC3198142.
990 12. Nakamura A, Hattori M, Sakaki Y. A novel gene isolated from human placenta
991 located in Down syndrome critical region on chromosome 21. DNA research : an
992 international journal for rapid publication of reports on genes and genomes. 1997;4(5):321-4.
993 doi: 10.1093/dnares/4.5.321. PubMed PMID: 9455479.
994 13. El Ghouzzi V. Mutations in the basic domain and the loop-helix II junction of TWIST
995 abolish DNA binding in Saethre-Chotzen syndrome. FEBS Lett. 2001;492:112-8.
996 14. Kamath BM, Stolle C, Bason L, Colliton RP, Piccoli DA, Spinner NB, et al.
997 Craniosynostosis in Alagille syndrome. Am J Med Genet. 2002;112(2):176-80. doi:
998 10.1002/ajmg.10608. PubMed PMID: 12244552.
999 15. Hood RL, Lines MA, Nikkel SM, Schwartzentruber J, Beaulieu C, Nowaczyk MJ, et
1000 al. Mutations in SRCAP, encoding SNF2-related CREBBP activator protein, cause Floating-
1001 Harbor syndrome. Am J Hum Genet. 2012;90(2):308-13. doi: 10.1016/j.ajhg.2011.12.001.
1002 PubMed PMID: 22265015; PubMed Central PMCID: PMC3276662.
1003 16. Roper RJ, Baxter LL, Saran NG, Klinedinst DK, Beachy PA, Reeves RH. Defective
1004 cerebellar response to mitogenic Hedgehog signaling in Down's syndrome mice. Proc Natl
1005 Acad Sci U S A. 2006;103(5):1452-6.
1006 17. Croonen EA, van der Burgt I, Kapusta L, Draaisma JM. Electrocardiography in
1007 Noonan syndrome PTPN11 gene mutation--phenotype characterization. American journal of
1008 medical genetics Part A. 2008;146A(3):350-3. doi: 10.1002/ajmg.a.32140. PubMed PMID:
1009 18203203.
1010 18. Fourie Z, Damstra J, Gerrits PO, Ren Y. Evaluation of anthropometric accuracy and
1011 reliability using different three-dimensional scanning systems. Forensic Sci Int. 2011;207(1-
1012 3):127-34. doi: 10.1016/j.forsciint.2010.09.018. PubMed PMID: 20951517.
1013 19. Toma AM, Zhurov A, Playle R, Ong E, Richmond S. Reproducibility of facial soft
1014 tissue landmarks on 3D laser-scanned facial images. Orthodontics & Craniofacial Research.
1015 2009;12(1):33-42. doi: 10.1111/j.1601-6343.2008.01435.x.
1016 20. Kovacs L, Zimmermann A, Brockmann G, Baurecht H, Schwenzer-Zimmerer K,
1017 Papadopulos NA, et al. Accuracy and Precision of the Three-Dimensional Assessment of the

1018 Facial Surface Using a 3-D Laser Scanner. IEEE Transactions on Medical Imaging.
1019 2006;25(6):742-54. PubMed PMID: 21197761.
1020 21. Coussens AK, Daal Av. Linkage disequilibrium analysis identifies an FGFR1
1021 haplotype-tag SNP associated with normal variation in craniofacial shape. Genomics.
1022 2005;85(5):563-73. doi: DOI: 10.1016/j.ygeno.2005.02.002.
1023 22. Paternoster L, Zhurov AI, Toma AM, Kemp JP, St Pourcain B, Timpson NJ, et al.
1024 Genome-wide association study of three-dimensional facial morphology identifies a variant
1025 in PAX3 associated with nasion position. Am J Hum Genet. 2012;90(3):478-85. Epub
1026 2012/02/22. doi: 10.1016/j.ajhg.2011.12.021. PubMed PMID: 22341974; PubMed Central
1027 PMCID: PMC3309180.
1028 23. Liu F, van der Lijn F, Schurmann C, Zhu G, Chakravarty MM, Hysi PG, et al. A
1029 genome-wide association study identifies five loci influencing facial morphology in
1030 Europeans. PLoS Genet. 2012;8(9):e1002932. doi: 10.1371/journal.pgen.1002932. PubMed
1031 PMID: 23028347; PubMed Central PMCID: PMC3441666.
1032 24. Michel S, Liang L, Depner M, Klopp N, Ruether A, Kumar A, et al. Unifying
1033 candidate gene and GWAS Approaches in Asthma. PLoS One. 2010;5(11):e13894. doi:
1034 10.1371/journal.pone.0013894. PubMed PMID: 21103062; PubMed Central PMCID:
1035 PMC2980484.
1036 25. Sun J, Jia P, Fanous AH, Webb BT, van den Oord EJ, Chen X, et al. A multi-
1037 dimensional evidence-based candidate gene prioritization approach for complex diseases-
1038 schizophrenia as a case. Bioinformatics. 2009;25(19):2595-6602. doi:
1039 10.1093/bioinformatics/btp428. PubMed PMID: 19602527; PubMed Central PMCID:
1040 PMC2752609.
1041 26. Hrdy DB. Analysis of hair samples of mummies from Semma South (Sudanese
1042 Nubia). Am J Phys Anthropol. 1978;49(2):277-82. doi: 10.1002/ajpa.1330490217. PubMed
1043 PMID: 717558.
1044 27. Fitzpatrick TB. The validity and practicality of sun-reactive skin types I through VI.
1045 Archives of Dermatology. 1988;124(6):869.
1046 28. Sturm RA, Larsson M. Genetics of human iris colour and patterns. Pigment Cell
1047 Melanoma Res. 2009;22(5):544-62. doi: 10.1111/j.1755-148X.2009.00606.x. PubMed
1048 PMID: 19619260.
1049 29. Farkas LG. Anthropometry of the head and face. 2nd ed. New York: Raven Press;
1050 1994. xix, 405 p. p.

1051 30. Site MMRW. The Jackson Laboratory, Bar Harbor, Maine. World Wide Web
1052 (http://mousemutant.jax.org/) Bar Harbor, Maine.2010 [cited 2013 March]. Available from:
1053 http://mousemutant.jax.org/.
1054 31. Ashburner M, Ball CA, Blake JA, Botstein D, Butler H, Cherry JM, et al. Gene
1055 ontology: tool for the unification of biology. The Gene Ontology Consortium. Nat Genet.
1056 2000;25(1):25-9. doi: 10.1038/75556. PubMed PMID: 10802651; PubMed Central PMCID:
1057 PMC3037419.
1058 32. Online Mendelian Inheritance in Man O. McKusick-Nathans Institute of Genetic
1059 Medicine, Johns Hopkins University (Baltimore, MD) [cited 2012 March]. Available from:
1060 http://omim.org/.
1061 33. Rebhan M, ChalifaCaspi V, Prilusky J, Lancet D. GeneCards: Integrating information
1062 about genes, proteins and diseases. Trends in Genetics. 1997;13(4):163-. doi: Doi
1063 10.1016/S0168-9525(97)01103-7. PubMed PMID: WOS:A1997WQ96900011.
1064 34. Sabeti PC, Varilly P, Fry B, Lohmueller J, Hostetter E, Cotsapas C, et al. Genome-
1065 wide detection and characterization of positive selection in human populations. Nature.
1066 2007;449(7164):913-8. doi: 10.1038/nature06250. PubMed PMID: 17943131; PubMed
1067 Central PMCID: PMC2687721.
1068 35. Zhou N, Wang L. Effective selection of informative SNPs and classification on the
1069 HapMap genotype data. BMC Bioinformatics. 2007;8(1):484. PubMed PMID:
1070 doi:10.1186/1471-2105-8-484.
1071 36. Kosoy R, Nassir R, Tian C, White PA, Butler LM, Silva G, et al. Ancestry
1072 informative marker sets for determining continental origin and admixture proportions in
1073 common populations in America. Hum Mutat. 2009;30(1):69-78. doi: 10.1002/humu.20822.
1074 PubMed PMID: 18683858; PubMed Central PMCID: PMC3073397.
1075 37. Paschou P, Lewis J, Javed A, Drineas P. Ancestry informative markers for fine-scale
1076 individual assignment to worldwide populations. Journal of Medical Genetics. doi:
1077 10.1136/jmg.2010.078212.
1078 38. Londin ER, Keller MA, Maista C, Smith G, Mamounas LA, Zhang R, et al. CoAIMs:
1079 a cost-effective panel of ancestry informative markers for determining continental origins.
1080 PLoS One. 2010;5(10):e13443. doi: 10.1371/journal.pone.0013443. PubMed PMID:
1081 20976178; PubMed Central PMCID: PMC2955551.
1082 39. Bulbul O, Filoglu G, Altuncul H, Aradas AF, Ruiz Y, Fondevila M, et al. A SNP
1083 multiplex for the simultaneous prediction of biogeographic ancestry and pigmentation type.
1084 Forensic Sci Inter: Genet Suppl. 2011;3(1):e500-e1. doi: 10.1016/j.fsigss.2011.10.001.

1085 40. Tandon A, Patterson N, Reich D. Ancestry informative marker panels for African
1086 Americans based on subsets of commercially available SNP arrays. Genet Epidemiol.
1087 2011;35(1):80-3. doi: 10.1002/gepi.20550. PubMed PMID: 21181899.
1088 41. Phillips C, Freire Aradas A, Kriegel AK, Fondevila M, Bulbul O, Santos C, et al.
1089 Eurasiaplex: a forensic SNP assay for differentiating European and South Asian ancestries.
1090 Forensic Sci Int Genet. 2013;7(3):359-66. doi: 10.1016/j.fsigen.2013.02.010. PubMed PMID:
1091 23537756.
1092 42. Gettings KB, Lai R, Johnson JL, Peck MA, Hart JA, Gordish-Dressman H, et al. A
1093 50-SNP assay for biogeographic ancestry and phenotype prediction in the U.S. population.
1094 Forensic Sci Int Genet. 2014;8(1):101-8. doi: 10.1016/j.fsigen.2013.07.010. PubMed PMID:
1095 24315596.
1096 43. Kidd KK, Speed WC, Pakstis AJ, Furtado MR, Fang R, Madbouly A, et al. Progress
1097 toward an efficient panel of SNPs for ancestry inference. Forensic Sci Int Genet.
1098 2014;10C(0):23-32. doi: 10.1016/j.fsigen.2014.01.002. PubMed PMID: 24508742.
1099 44. Amigo J, Salas A, Phillips C. ENGINES: exploring single nucleotide variation in
1100 entire human genomes. BMC Bioinformatics. 12(1):105. PubMed PMID: doi:10.1186/1471-
1101 2105-12-105.
1102 45. Adzhubei IA, Schmidt S, Peshkin L, Ramensky VE, Gerasimova A, Bork P, et al. A
1103 method and server for predicting damaging missense mutations. Nat Methods. 2010;7(4):248-
1104 9. doi: 10.1038/nmeth0410-248. PubMed PMID: 20354512; PubMed Central PMCID:
1105 PMC2855889.
1106 46. Marinescu V, Kohane I, Riva A. MAPPER: a search engine for the computational
1107 identification of putative transcription factor binding sites in multiple genomes. BMC
1108 Bioinformatics. 2005;6(1):79. PubMed PMID: doi:10.1186/1471-2105-6-79.
1109 47. Wang J, Ronaghi M, Chong SS, Lee CGL. pfSNP: An integrated potentially
1110 functional SNP resource that facilitates hypotheses generation through knowledge syntheses.
1111 Human Mutation. 32(1):19-24. doi: 10.1002/humu.21331.
1112 48. Coassin S, Brandstätter A, Kronenberg F. Lost in the space of bioinformatic tools: A
1113 constantly updated survival guide for genetic epidemiology. The GenEpi Toolbox.
1114 Atherosclerosis. 209(2):321-35. doi: DOI: 10.1016/j.atherosclerosis.2009.10.026.
1115 49. Pritchard JK, Stephens M, Donnelly P. Inference of population structure using
1116 multilocus genotype data. Genetics. 2000;155(2):945-59. PubMed PMID:
1117 WOS:000087475100039.

1118 50. Thorisson G, Smith A, Krishnan L, Stein L. The International HapMap Project Web
1119 site. Genome Res. 2005;15:1592.
1120 51. Purcell S, Neale B, Todd-Brown K, Thomas L, Ferreira MA, Bender D, et al. PLINK:
1121 a tool set for whole-genome association and population-based linkage analyses. Am J Hum
1122 Genet. 2007;81(3):559-75. doi: 10.1086/519795. PubMed PMID: 17701901; PubMed Central
1123 PMCID: PMC1950838.
1124 52. Price AL, Patterson NJ, Plenge RM, Weinblatt ME, Shadick NA, Reich D. Principal
1125 components analysis corrects for stratification in genome-wide association studies. Nat
1126 Genet. 2006;38(8):904-9. doi: 10.1038/ng1847. PubMed PMID: 16862161.
1127 53. Patterson N, Price AL, Reich D. Population structure and eigenanalysis. PLoS Genet.
1128 2006;2(12):e190. doi: 10.1371/journal.pgen.0020190. PubMed PMID: 17194218; PubMed
1129 Central PMCID: PMC1713260.
1130 54. UniProt C. Activities at the Universal Protein Resource (UniProt). Nucleic Acids Res.
1131 2014;42(Database issue):D191-8. doi: 10.1093/nar/gkt1140. PubMed PMID: 24253303;
1132 PubMed Central PMCID: PMC3965022.
1133 55. Rappaport N, Nativ N, Stelzer G, Twik M, Guan-Golan Y, Stein TI, et al. MalaCards:
1134 an integrated compendium for diseases and their annotation. Database : the journal of
1135 biological databases and curation. 2013;2013:bat018. doi: 10.1093/database/bat018. PubMed
1136 PMID: 23584832; PubMed Central PMCID: PMC3625956.
1137 56. Warde-Farley D, Donaldson SL, Comes O, Zuberi K, Badrawi R, Chao P, et al. The
1138 GeneMANIA prediction server: biological network integration for gene prioritization and
1139 predicting gene function. Nucleic Acids Res. 2010;38(Web Server issue):W214-20. doi:
1140 10.1093/nar/gkq537. PubMed PMID: 20576703; PubMed Central PMCID: PMC2896186.
1141 57. Reference Genome Group of the Gene Ontology C. The Gene Ontology's Reference
1142 Genome Project: a unified framework for functional annotation across species. PLoS Comput
1143 Biol. 2009;5(7):e1000431. doi: 10.1371/journal.pcbi.1000431. PubMed PMID: 19578431;
1144 PubMed Central PMCID: PMC2699109.
1145 58. Sherry ST, Ward MH, Kholodov M, Baker J, Phan L, Smigielski EM, et al. dbSNP:
1146 the NCBI database of genetic variation. Nucleic Acids Research. 2001;29(1):308-11. doi:
1147 10.1093/nar/29.1.308.
1148 59. Durbin RM, Abecasis GR, Altshuler DL, Auton A, Brooks LD, Gibbs RA, et al. A
1149 map of human genome variation from population-scale sequencing. Nature. 467(7319):1061 -
1150 73. PubMed PMID: doi:10.1038/nature09534.

1151 60. Chelala C, Khan A, Lemoine NR. SNPnexus: a web database for functional
1152 annotation of newly discovered and public domain single nucleotide polymorphisms.
1153 Bioinformatics. 2009;25(5):655-61. doi: 10.1093/bioinformatics/btn653. PubMed PMID:
1154 19098027; PubMed Central PMCID: PMC2647830.
1155 61. Rajeevan H, Cheung KH, Gadagkar R, Stein S, Soundararajan U, Kidd JR, et al.
1156 ALFRED: an allele frequency database for microevolutionary studies. Evol Bioinform
1157 Online. 2005;1:1-10. PubMed PMID: 19325849; PubMed Central PMCID: PMC2658869.
1158 62. Johnson AD, Handsaker RE, Pulit SL, Nizzari MM, O'Donnell CJ, de Bakker PI.
1159 SNAP: a web-based tool for identification and annotation of proxy SNPs using HapMap.
1160 Bioinformatics. 2008;24(24):2938-9. doi: 10.1093/bioinformatics/btn564. PubMed PMID:
1161 18974171; PubMed Central PMCID: PMC2720775.
1162 63. Boyle AP, Hong EL, Hariharan M, Cheng Y, Schaub MA, Kasowski M, et al.
1163 Annotation of functional variation in personal genomes using RegulomeDB. Genome Res.
1164 2012;22(9):1790-7. doi: 10.1101/gr.137323.112. PubMed PMID: 22955989; PubMed Central
1165 PMCID: PMC3431494.
1166 64. Aung SC, Ngim RC, Lee ST. Evaluation of the laser scanner as a surface measuring
1167 tool and its accuracy compared with direct facial anthropometric measurements. British
1168 journal of plastic surgery. 1995;48(8):551-8. PubMed PMID: 8548155.
1169 65. Bianchi SD, Spada MC, Bianchi L, VerzÃ¨ L, Vezzetti E, Tornincasa S, et al.
1170 Evaluation of scanning parameters for a surface colour laser scanner. International Congress
1171 Series. 2004;1268:1162-7. doi: 10.1016/j.ics.2004.03.264. PubMed PMID: 13327565.
1172 66. Kusnoto B, Evans CA. Reliability of a 3D surface laser scanner for orthodontic
1173 applications. American journal of orthodontics and dentofacial orthopedics : official
1174 publication of the American Association of Orthodontists, its constituent societies, and the
1175 American Board of Orthodontics. 2002;122(4):342-8. PubMed PMID: 12411877.
1176 67. Ma L, Xu T, Lin J. Validation of a three-dimensional facial scanning system based on
1177 structured light techniques. Computer Methods & Programs in Biomedicine. 2009;94(3):290-
1178 8. doi: 10.1016/j.cmpb.2009.01.010. PubMed PMID: 37572488.
1179 68. Gwilliam JR, Cunningham SJ, Hutton T. Reproducibility of soft tissue landmarks on
1180 three-dimensional facial scans. European journal of orthodontics. 2006;28(5):408-15. doi:
1181 10.1093/ejo/cjl024. PubMed PMID: 16901962.
1182 69. McLean CY, Bristor D, Hiller M, Clarke SL, Schaar BT, Lowe CB, et al. GREAT
1183 improves functional interpretation of cis-regulatory regions. Nat Biotechnol. 2010;28(5):495-
1184 501. doi: 10.1038/nbt.1630. PubMed PMID: 20436461.

1185 70. Weston EM, Friday AE, Lio P. Biometric evidence that sexual selection has shaped
1186 the hominin face. PLoS One. 2007;2(8):e710. doi: 10.1371/journal.pone.0000710. PubMed
1187 PMID: 17684556; PubMed Central PMCID: PMC1937021.
1188 71. Cooper RS, Tayo B, Zhu X. Genome-wide association studies: implications for
1189 multiethnic samples. Hum Mol Genet. 2008;17(R2):R151-5. Epub 2008/10/15. doi:
1190 10.1093/hmg/ddn263. PubMed PMID: 18852204; PubMed Central PMCID: PMC2782359.
1191 72. Barnholtz-Sloan JS, Chakraborty R, Sellers TA, Schwartz AG. Examining population
1192 stratification via individual ancestry estimates versus self-reported race. Cancer Epidemiol
1193 Biomarkers Prev. 2005;14(6):1545-51. doi: 10.1158/1055-9965.EPI-04-0832. PubMed
1194 PMID: 15941970.
1195 73. Tang H, Quertermous T, Rodriguez B, Kardia SL, Zhu X, Brown A, et al. Genetic
1196 structure, self-identified race/ethnicity, and confounding in case-control association studies.
1197 Am J Hum Genet. 2005;76(2):268-75. doi: 10.1086/427888. PubMed PMID: 15625622;
1198 PubMed Central PMCID: PMC1196372.
1199 74. Price AL, Zaitlen NA, Reich D, Patterson N. New approaches to population
1200 stratification in genome-wide association studies. Nat Rev Genet. 2010;11(7):459-63. Epub
1201 2010/06/16. doi: 10.1038/nrg2813. PubMed PMID: 20548291; PubMed Central PMCID:
1202 PMC2975875.
1203 75. Panagiotou OA, Ioannidis JP, Genome-Wide Significance P. What should the
1204 genome-wide significance threshold be? Empirical replication of borderline genetic
1205 associations. International journal of epidemiology. 2012;41(1):273-86. doi:
1206 10.1093/ije/dyr178. PubMed PMID: 22253303.
1207 76. Dudbridge F, Gusnanto A. Estimation of significance thresholds for genomewide
1208 association scans. Genet Epidemiol. 2008;32(3):227-34. doi: 10.1002/gepi.20297. PubMed
1209 PMID: 18300295; PubMed Central PMCID: PMC2573032.
1210 77. Attanasio C, Nord AS, Zhu Y, Blow MJ, Li Z, Liberton DK, et al. Fine tuning of
1211 craniofacial morphology by distant-acting enhancers. Science. 2013;342(6157):1241006. doi:
1212 10.1126/science.1241006. PubMed PMID: 24159046.
1213 78. Thomas PD, Campbell MJ, Kejariwal A, Mi H, Karlak B, Daverman R, et al.
1214 PANTHER: a library of protein families and subfamilies indexed by function. Genome Res.
1215 2003;13(9):2129-41. doi: 10.1101/gr.772403. PubMed PMID: 12952881; PubMed Central
1216 PMCID: PMC403709.
1217 79. Goymer P. Synonymous mutations break their silence. Nat Rev Genet. 2007;8(2):92-.

1218 80. Zhao Y, Guo YJ, Tomac AC, Taylor NR, Grinberg A, Lee EJ, et al. Isolated cleft
1219 palate in mice with a targeted mutation of the LIM homeobox gene lhx8. Proc Natl Acad Sci
1220 U S A. 1999;96(26):15002-6. PubMed PMID: 10611327; PubMed Central PMCID:
1221 PMC24762.
1222 81. Zhang Y, Mori T, Takaki H, Takeuch M, Iseki K, Hagino S, et al. Comparison of the
1223 expression patterns of two LIM-homeodomain genes, Lhx6 and L3/Lhx8, in the developing
1224 palate. Orthod Craniofac Res. 2002;5(2):65-70. PubMed PMID: 12086327.
1225 82. Galdzicka M, Patnala S, Hirshman MG, Cai JF, Nitowsky H, A Egeland J, et al. A
1226 new gene, EVC2, is mutated in Ellis–van Creveld syndrome. Molecular genetics and
1227 metabolism. 2002;77(4):291-5. doi: 10.1016/s1096-7192(02)00178-6.
1228 83. Novelli G, Muchir A, Sangiuolo F, Helbling-Leclerc A, D'Apice MR, Massart C, et
1229 al. Mandibuloacral dysplasia is caused by a mutation in LMNA-encoding lamin A/C. Am J
1230 Hum Genet. 2002;71(2):426-31. doi: 10.1086/341908. PubMed PMID: 12075506; PubMed
1231 Central PMCID: PMC379176.
1232 84. Abdelhak S, Kalatzis V, Heilig R, Compain S, Samson D, Vincent C, et al. A human
1233 homologue of the Drosophila eyes absent gene underlies branchio-oto-renal (BOR) syndrome
1234 and identifies a novel gene family. Nat Genet. 1997;15(2):157-64. doi: 10.1038/ng0297-157.
1235 PubMed PMID: 9020840.

1236 85. Poliseno L, Salmena L, Zhang J, Carver B, Haveman WJ, Pandolfi PP. A coding-
1237 independent function of gene and pseudogene mRNAs regulates tumour biology. Nature.
1238 2010;465(7301):1033-8.
1239 86. Hirotsune S, Yoshida N, Chen A, Garrett L, Sugiyama F, Takahashi S, et al. An
1240 expressed pseudogene regulates the messenger-RNA stability of its homologous coding gene.
1241 Nature. 2003;423(6935):91-6.
1242 87. Allache R, De Marco P, Merello E, Capra V, Kibar Z. Role of the planar cell polarity
1243 gene CELSR1 in neural tube defects and caudal agenesis. Birth defects research Part A,
1244 Clinical and molecular teratology. 2012;94(3):176-81. doi: 10.1002/bdra.23002. PubMed
1245 PMID: 22371354.
1246 88. Meng Q, Jin C, Chen Y, Chen J, Medvedovic M, Xia Y. Expression of signaling
1247 components in embryonic eyelid epithelium. PLoS One. 2014;9(2):e87038. doi:
1248 10.1371/journal.pone.0087038. PubMed PMID: 24498290; PubMed Central PMCID:
1249 PMC3911929.

1250 89. Visscher PM. Sizing up human height variation. Nature Genetics. 2008;40(5):489-90.
1251 doi: 10.1038/ng0508-489. PubMed PMID: 18443579.
1252 90. Wood AR, Esko T, Yang J, Vedantam S, Pers TH, Gustafsson S, et al. Defining the
1253 role of common variation in the genomic and biological architecture of adult human height.
1254 Nat Genet. 2014;46(11):1173-86. doi: 10.1038/ng.3097. PubMed PMID: 25282103; PubMed
1255 Central PMCID: PMCPMC4250049.

1256 91. Claes P, Liberton DK, Daniels K, Rosana KM, Quillen EE, Pearson LN, et al. Modeling
1257 3D facial shape from DNA. PLoS Genet. 2014;10(3):e1004224. doi:
1258 10.1371/journal.pgen.1004224. PubMed PMID: 24651127; PubMed Central PMCID:
1259 PMC3961191.
1260 92. Lau E. Non-coding RNA: Zooming in on lncRNA functions. Nat Rev Genet.
1261 2014;15(9):574-5. doi: 10.1038/nrg3795.
1262 93. Wu H, Nord AS, Akiyama JA, Shoukry M, Afzal V, Rubin EM, et al. Tissue-Specific
1263 RNA Expression Marks Distant-Acting Developmental Enhancers. PLoS Genet.
1264 2014;10(9):e1004610. doi: 10.1371/journal.pgen.1004610.
1265 94. Peng S, Tan J, Hu S, Zhou H, Guo J, Jin L, et al. Detecting Genetic Association of
1266 Common Human Facial Morphological Variation Using High Density 3D Image
1267 Registration. PLoS Comput Biol. 2013;9(12):e1003375. doi: 10.1371/journal.pcbi.100337.
1268 95. Wolf L, Donner Y, editors. An experimental study of employing visual appearance as
1269 a phenotype. Computer Vision and Pattern Recognition, 2008 CVPR 2008 IEEE Conference
1270 on; 2008: IEEE.
1271 96. Claes P, Hill H, Shriver MD. Toward DNA-based facial composites: preliminary
1272 results and validation. Forensic Sci Int Genet. 2014;13:208-16. doi:
1273 10.1016/j.fsigen.2014.08.008. PubMed PMID: 25194685.

Figure legends and additional file descriptions

Figure 1. **Anatomical position of the 32 manually annotated anthropometric landmarks used for calculation of linear and angular distances and ratios between the linear distances.** Some landmarks are not clearly visible due to image orientation. gn = Gnathion, pg= Pogonion, sl = Sublabiale, li = Labiale Inferius, sto = Stomion, ls = Labiale superius, ch-r = Chelion right, ch-l = Chelion left, go-r = Gonion Right, go-l = Gonion left, sn = Subnasale, prn= Pronasale, al-r = Alare right; al-l= Alare left, n = Nasion, g= Glabella; tr = Tragion, en-l = left Endocanthion, en-r = right Endocanthion, ex-r = Right Endocanthion; ex-l = left Endocanthion, ps-r = Palpebrale superius right, ps-l = Palpebrale superius left , pi-r = Palpebrale inferius right, pi-l = Palpebrale inferius left, zy-r = Zygion Right, zy-l = Zygion Left, pra-r = Tragion right, pra-l = Tragion Left, sba-l = Subalare left, sa-l = Superaurale Left, pa-l = Postaurale left.

Figure 2. Illustration of linear and angular distances calculated from manually annotated landmark coordinates.

Figure 3. Population structure as represented by plotting genomic PCs 1 and 2, using 270 HapMap individuals as anchor clusters. YRI: Yoruba, Nigeria, Africa. JRI: Japanese, Tokyo, Japan. CHB: Han Chinese, Beijing, China. CEU: Utah residents with European ancestry.

Additional files

Figure S1. Q-Q plot of the PCA-corrected −log10 p-values for the difference between the observed association for the tails of al-al distance and expected association based on the overall al-al distance distribution.

Figure S2. Q-Q plot of the PCA-corrected −log10 p-values for the difference between the observed association for the tails of sn-prn distance and expected association based on the overall sn-prn distance distribution.

Figure S3. Q-Q plot of the PCA-corrected −log10 p-values for the difference between the observed association for the tails of cephalic index and expected association based on the overall cephalic index distribution.

Figure S4. Q-Q plot of the PCA-corrected −log10 p-values for the difference between the observed association for the tails of nasal index and expected association based on the overall nasal index distribution.

Figure S5. Q-Q plot of the PCA-corrected −log10 p-values for the difference between the observed association for the tails of nose-face width index and expected association based on the overall nose-face width index distribution.

Figure S6. Q-Q plot of the PCA-corrected −log10 p-values for the difference between the observed association for the tails of nasolabial angle and expected association based on the overall nasolabial angle distance distribution.

Figure S7. Q-Q plot of the PCA-corrected −log10 p-values for the difference between the observed association for the tails of transverse nasal prominence angle and expected association based on the overall transverse nasal prominence angle distribution.

Figure S8. Q-Q plot of the PCA-corrected −log10 p-values for the difference between the observed association for the tails of PC1 trait and expected association based on the overall PC1 trait distance distribution.

Figure S9. Manhattan plot of the genomic associations of the al-al distance, based on the initial p-values from analysis of the PCA-corrected data. The −log10 (P value) is plotted against the physical positions of each SNP on each chromosome. The basic significance threshold is indicated by the blue line for -log10(1e-5) and the genome-wide significance threshold for -log10(5e-8) is indicated by the red line.

Figure S10. Manhattan plot of the genomic associations of the sn-prn distance, based on the initial p-values from analysis of the PCA-corrected data. The −log10 (P value) is plotted against the physical positions of each SNP on each chromosome. The basic significance threshold is indicated by the blue line for -log10(1e-5) and the genome-wide significance threshold for -log10(5e-8) is indicated by the red line.

Figure S11. Manhattan plot of the genomic associations of the cephalic index, based on the initial p-values from analysis of the PCA-corrected data. The −log10 (P value) is plotted against the physical positions of each SNP on each chromosome. The basic significance threshold is indicated by the blue line for -log10(1e-5) and the genome-wide significance threshold for -log10(5e-8) is indicated by the red line.

Figure S12. Manhattan plot of the genomic associations of the nasal index, based on the initial p-values from analysis of the PCA-corrected data. The

−log10 (P value) is plotted against the physical positions of each SNP on each chromosome. The basic significance threshold is indicated by the blue line for -log10(1e-5) and the genome-wide significance threshold for -log10(5e-8) is indicated by the red line.

Figure S13. Manhattan plot of the genomic associations of the nose-face width index, based on the initial p-values from analysis of the PCA-corrected data. The −log10 (P value) is plotted against the physical positions of each SNP on each chromosome. The basic significance threshold is indicated by the blue line for -log10(1e-5) and the genome-wide significance threshold for -log10(5e-8) is indicated by the red line.

Figure S14. Manhattan plot of the genomic associations of the nasolabial angle, based on the initial p-values from analysis of the PCA-corrected data. The −log10 (P value) is plotted against the physical positions of each SNP on each chromosome. The basic significance threshold is indicated by the blue line for -log10(1e-5) and the genome-wide significance threshold for -log10(5e-8) is indicated by the red line.

Figure S15. Manhattan plot of the genomic associations of the transverse nasal prominence angle, based on the initial p-values from analysis of the PCA-corrected data. The −log10 (P value) is plotted against the physical positions of each SNP on each chromosome. The basic significance threshold is indicated by the blue line for -log10(1e-5) and the genome-wide significance threshold for -log10(5e-8) is indicated by the red line.

Figure S16. Manhattan plot of the genomic associations of the PC1 trait, based on the initial p-values from analysis of the PCA-corrected data. The −log10 (P value) is plotted against the physical positions of each SNP on each chromosome. The basic significance threshold is indicated by the blue line for -log10(1e-5) and the genome-wide significance threshold for -log10(5e-8) is indicated by the red line.

Figure S17. Pie chart, illustrating molecular function classification of human genes, harbouring genomic markers in significant association with craniofacial phenotypes. The genes include: *AGXT2*, *BMP4*, *CACNB4*, *COL11A1*, *EGFR*, *EYA1*, *EYA2*, *FAM49A*, *FOXN3*, *LMNA*, *MYO5A*, *PAX3*, *PCDH15*, *RTTN*, *SMAD1*, *XXYLT1* and *ZEB1*.

Figure S18. Pie chart, illustrating biological processes classification involving human genes, harbouring genomic markers in significant association with craniofacial phenotypes. The genes include: *AGXT2*, *BMP4*, *CACNB4*, *COL11A1*, *EGFR*, *EYA1*, *EYA2*, *FAM49A*, *FOXN3*, *LMNA*, *MYO5A*, *PAX3*, *PCDH15*, *RTTN*, *SMAD1*, *XXYLT1* and *ZEB1*.

Figure S19. Pie chart, illustrating protein product classification of the human genes, harbouring genomic markers in significant association with craniofacial phenotypes. The genes are: *AGXT2*, *BMP4*, *CACNB4*, *COL11A1*, *EGFR*, *EYA1*, *EYA2*, *FAM49A*, *FOXN3*, *LMNA*, *MYO5A*, *PAX3*, *PCDH15*, *RTTN*, *SMAD1*, *XXYLT1* and *ZEB1*.

Table S1. Manually annotated facial landmarks used in the study.

Table S2. Genetic associations with pigmentation traits. Gene: gene name; rs#: reference SNP ID number; SNP: chromosomal location of the marker; Genomic annotation: genomic location of the marker; UNADJ: Unadjusted p-values; BONF: Bonferroni single-step adjusted; HOLM: Holm (1979) step-down adjusted; SIDAK_SS: Sidak single-step adjusted; SIDAK_SD: Sidak step-down adjusted; FDR_BH: Benjamini & Hochberg (1995) step-up FDR control; FDR_BY: Benjamini & Yekutieli (2001) step-up FDR control.

Table S3. Genetic syndromes displaying various craniofacial abnormalities, used to locate candidate genes for the study.

Appendix S1. **Comprehensive list of web resources used for candidate gene search and its output**. Note the presence of multiple tabs in this spreadsheet.

Appendix S2. Three spreadsheets, detailing a list of 8,518 genetic markers genotyped in 587 DNA samples and a list of 2,332 markers used for association analyses, following MAF (2%) and HWE filtering.

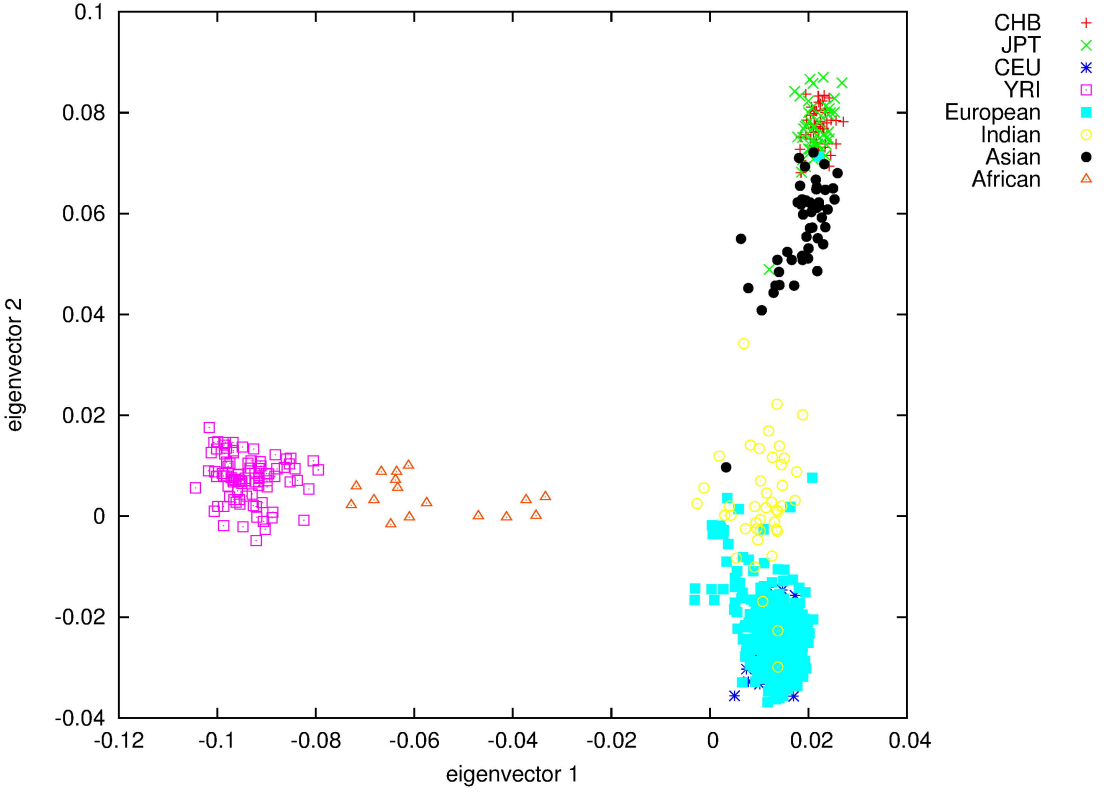
0.1
0.08
0.06
0.04
0.02
0
-0.02
-0.04
eigenvector 2
-0.12
-0.1
-0.08
-0.06
-0.04
-0.02
0
0.02
0.04
eigenvector 1
CHB
JPT
CEU
YRI
European
Indian
Asian
African

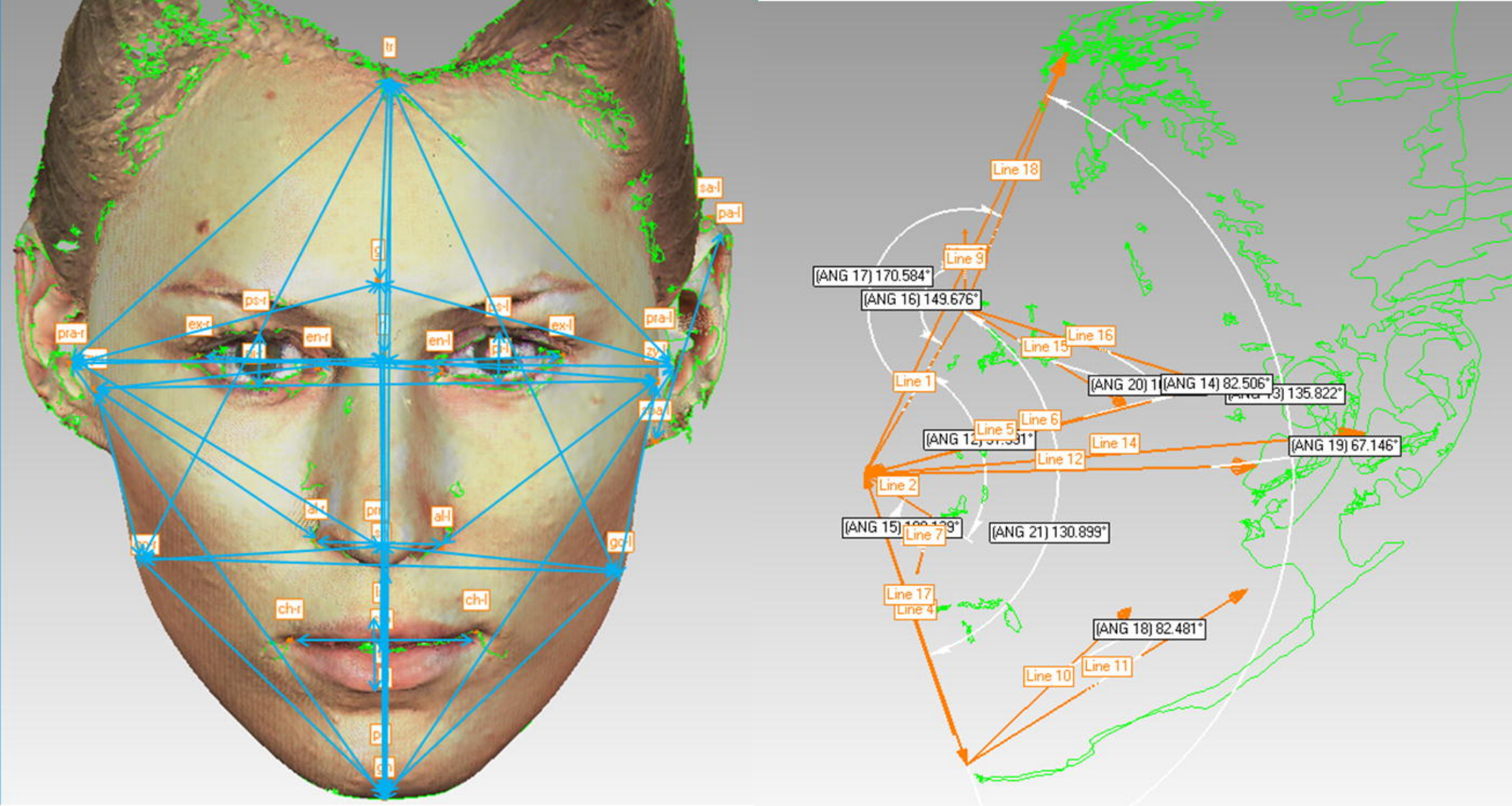
Line 18
Line 9
(ANG 17) 170.584°
(ANG 16) 149.676°
Line 16
Line 15
Line 1
(ANG 14) 82.506°
Line 6
Line 5
Line 14
Line 12
(ANG 19) 67.146°
Line 2
(ANG 21) 130.899°
Line 7
Line 17
Line 4
(ANG 18) 82.481°
Line 10
Line 11

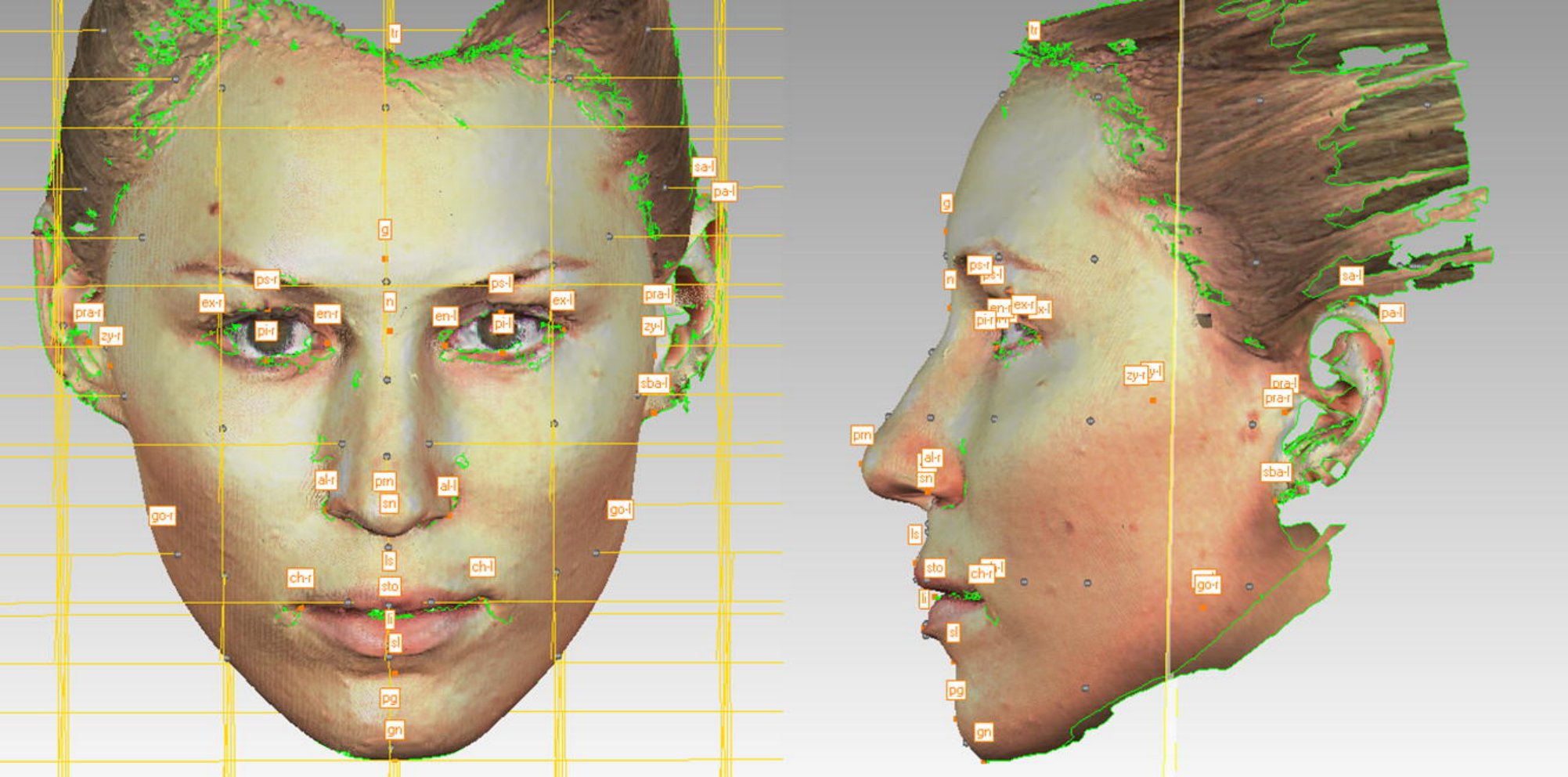
tr
sa-l
pa-l
g
ps-r
ps-l
ex-r
n
ex-l
pra-r
en-r
en-l
pra-l
pi-r
pi-l
zy-r
zy-l
sba-l
al-r
prn
al-l
sn
go-r
go-l
ls
ch-r
ch-l
sto
li
sl
pg
gn